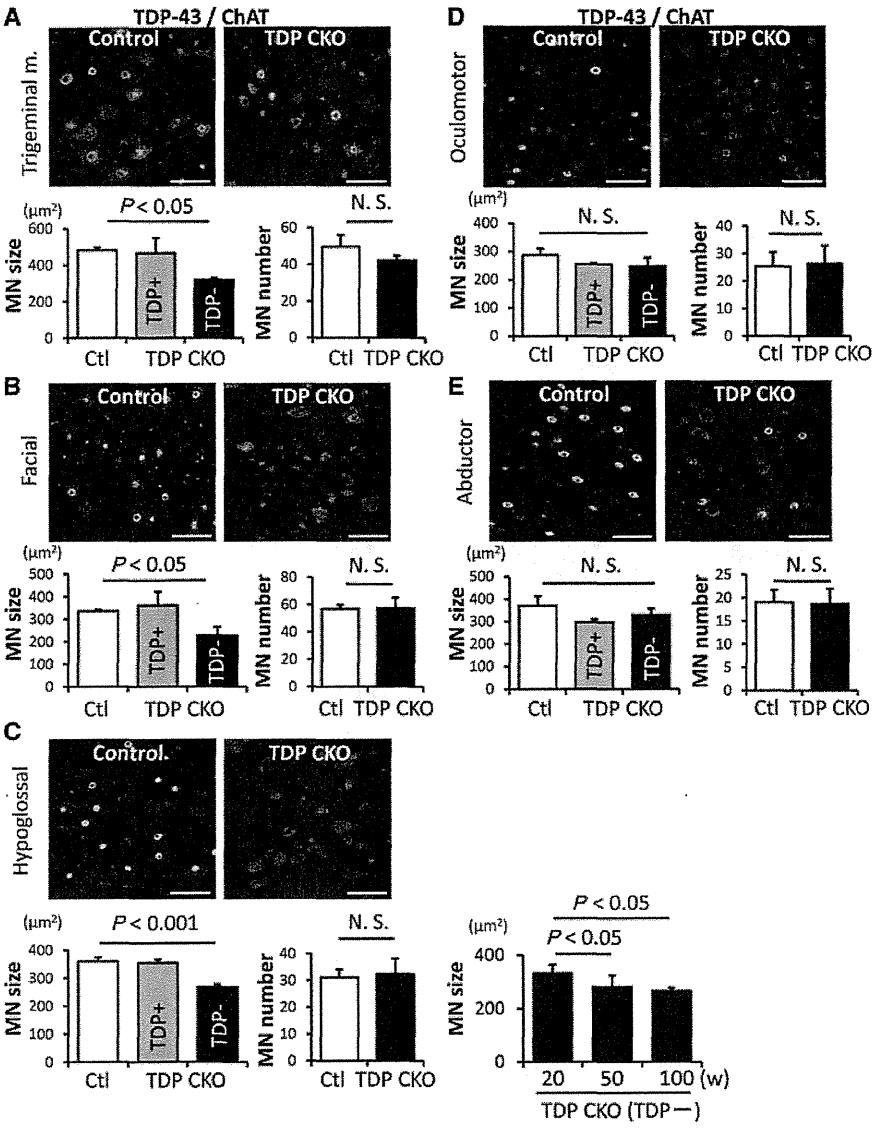

Figure 4 Morphological analysis of cranial motor nuclei. (**A–E**) Immunofluorescent analysis (TDP-43, green; ChAT, red) of motor neurons in the trigeminal motor (m.) (**A**), facial (**B**), hypoglossal (**C**), oculomotor (**D**), and abductor (**E**) nuclei from 100-week-old control ($n = 3$) and TDP CKO mice ($n = 3$). Graphs show the average size and number of motor neurons in each area. TDP+ = TDP-43-positive neuron; TDP− = TDP-43-negative neuron. Error bars indicate SD. Scale bars = 50 μm. MN = motor neuron; N.S. = not significant.

role of TDP-43 in postnatal mammalian neurons has not been fully elucidated. In the present study, we clarified that TDP CKO mice, in which TDP-43 was specifically knocked-out by Cre recombinase in postnatal motor neurons, develops a progressive motor neuronal degeneration as seen in ALS, suggesting that TDP-43 is essential for the long term maintenance of postnatal motor neurons in mice. Although TDP CKO mice developed ALS-like motor impairment, the mortality of the mice was not different from that of control littermates. This might be due to the knockout efficiency of TDP-43, which occurred in ~50% of motor neurons, or due to the life span of mice, which is considerably shorter than the disease duration of patients with ALS. Moreover, there were no significant alterations in body weight, motor function or morphology of motor neurons in our TDP heterozygous CKO (TDP hCKO) mice. Because previous studies demonstrated that the protein expression of TDP-43 was not reduced in various tissues of heterozygous TDP-43 knockout mice (Kraemer *et al.*, 2010; Sephton *et al.*, 2010; Wu *et al.*, 2010), TDP-43 depletion is likely insufficient to affect the motor neurons in our TDP hCKO mice. At the same time, these data suggest that expression of Cre itself did not affect the vulnerability of the mouse motor neurons over 2 years.

An earlier study demonstrates that the motor neuron-specific TDP-43 knockout mouse carrying HB9-Cre exhibits early-onset

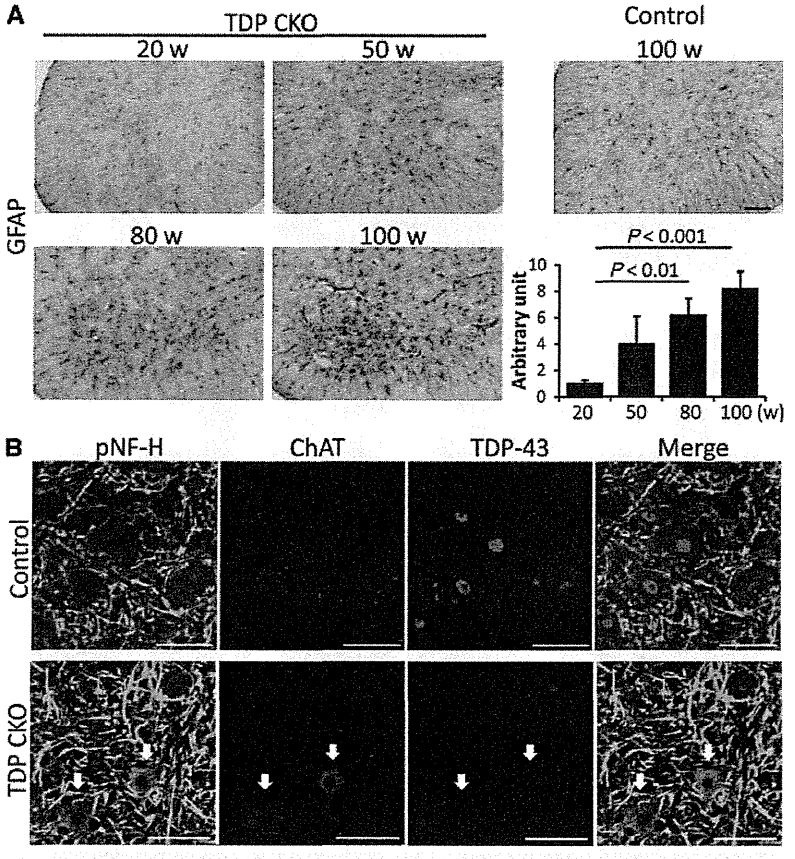

Figure 5 Astrogliosis and neuronal accumulation of phosphorylated neurofilament. (**A**) Immunohistochemistry against GFAP in the ventral horn and a time course analysis of astrogliosis. Error bars indicate SD ($n = 3$ for each age). (**B**) Immunofluorescent staining against pNF-H (green), ChAT (red) and TDP-43 (blue). pNF-H was accumulated in the cell bodies of TDP-43-lacking motor neurons of TDP CKO mice (arrows). Scale bars: **A** = 100 μm; **B** = 50 μm.

motor dysfunction and develops motor neuronal loss earlier than 10 weeks of age (Wu *et al.*, 2012). However, given that the Cre-mediated recombination using the *HB9* promoter began at the developmental stage E9.5 (Arber *et al.*, 1999), this model possibly reflects the loss-of-function of TDP-43 in the motor neuron development. By contrast, because the Cre expression in VAChT-Cre.Fast mice is mediated by the VAChT promoter, the number of Cre-expressing motor neurons in VAChT-Cre.Fast mice is scarcely detected at prenatal stages, but becomes maximum in number at 5 weeks (Misawa *et al.*, 2003). We also confirmed that TDP-43 was not excised in spinal motor neurons of TDP CKO mice at post-natal Day 2, but knocked-out in ~50 % of motor neurons of the 10-week-old mice. This temporal pattern of Cre expression appears to contribute to the late-onset progressive motor dysfunction in our TDP CKO mice and enable the assessment of loss of TDP-43 functions in mouse motor neurons at the postnatal stage. As far as we investigated, TDP-43 was knocked-out in spinal motor neurons beginning at 10 weeks, but the function and morphology of motor neurons were unexpectedly preserved for 1 year in TDP CKO mice, suggesting that the loss of TDP-43 was compensated in motor neurons of young mice, but triggered neuronal vulnerability with the ageing process. Given that ALS is an age-related neurodegenerative disease and that the disease develops after middle age even in inherited cases with TDP-43 mutations (Gitcho *et al.*, 2008; Kabashi *et al.*, 2008; Sreedharan *et al.*, 2008; Yokoseki *et al.*, 2008), our TDP CKO mice appear to be a model that recapitulates the age-dependent phenotypes of ALS. However, as TDP CKO mice lack some aspects of human ALS pathology, such as cytoplasmic inclusions of TDP-43 and the involvement of upper motor neurons, the use of this model for therapeutic research needs further validation.

In the histopathological analyses, TDP CKO mice exhibited the atrophy of motor neurons, degeneration of large motor axons, denervation of neuromuscular junctions and grouped atrophy of skeletal muscles, all of which are common to the pathology of human motor neuron disease. The disruption of retrograde labelling in TDP-43-lacking motor neurons suggests that TDP-43 depletion directly induces neuronal dysfunction. Interestingly, the axonal degenerations were evident in the ventral root of TDP CKO mice at 50 weeks of age, when the morphology of lumbar motor neurons was not altered. These findings are compatible with the fact that ALS pathology initially manifests at the axon

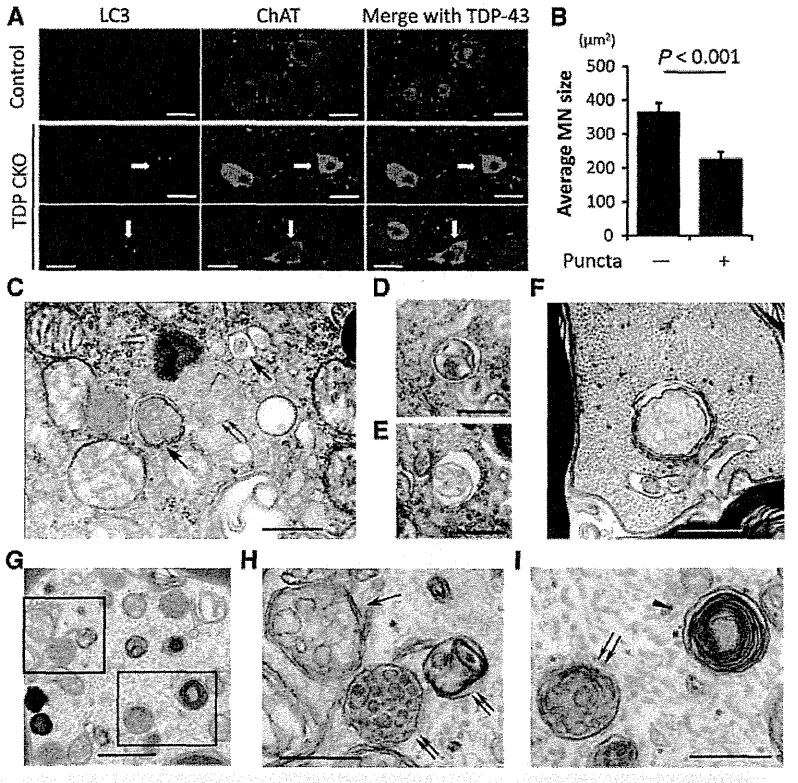

Figure 6 Formation of autophagosomes in motor neurons of TDP CKO mice. (**A**) Immunofluorescent analysis (LC3, green; ChAT, red; TDP-43, blue) revealed LC3-positive cytoplasmic puncta in TDP-43-lacking motor neurons of 100-week-old TDP CKO mice. (**B**) The average size of TDP-43 lacking motor neurons (MN) with ($n = 25$) and without ($n = 48$) LC3-positive puncta. Error bars indicate SEM. (**C–I**) Ultrastructural analysis of 100-week-old TDP CKO mice. Autophagosomes (arrows) and an autolysosome (double arrows) (**C**), autolysosomes surrounded by a single membrane containing mitochondria (**D**) and autophagosomes containing ribosome-like structures (**E**) were observed in the cell bodies of the motor neurons. An autophagic structure in the proximal motor axon (**F**). Accumulation of organelles containing mitochondria, autophagosomes (arrows), autolysosomes (double arrows), and autophagic structure with a multi-lamelleted structure (arrowhead) in the sciatic nerve (**G**) and its enlarged images (**D**, **E**, **H** and **I**). Scale bars: **A** = 20 μm; **C** and **G** = 1 μm; **F**, **H** and **I** = 500 nm.

(Fischer *et al.*, 2004). The increase of small myelinated fibres accompanied by the decrease of large myelinated fibres in the ventral root of 100-week-old TDP CKO mice corresponds to the morphological change in the cell body of the motor neurons, and similar observations were also reported in the patients and mouse models of ALS (Bradley *et al.*, 1983; Zhang *et al.*, 1997). TDP CKO mice also exhibited several features that are shared with patients with sporadic ALS: the involvement in the cranial motor nuclei such as the hypoglossal nucleus, preserved morphology in the extraocular motor neurons, accumulations of phosphorylated neurofilament in motor neurons and astrogliosis in the spinal ventral horn. Dysphagia due to the involvement of the hypoglossal nucleus might enhance the weight loss in aged TDP CKO mice through decreased oral intake. In ALS, extraocular motor neurons are resistant to degeneration compared with other somatomotor neurons, and differences in calcium buffering capacities have been proposed as a possible reason for this selective vulnerability (Alexianu *et al.*, 1994; Reiner *et al.*, 1995; Laslo *et al.*, 2000). Because RNA-seq analysis demonstrates that depletion of TDP-43 affects the calcium signalling pathway in mouse striatum (Polymenidou *et al.*, 2011), it is possible that dysregulation of calcium buffering underlies the pathogenesis of TDP CKO mice.

Our immunofluorescent analysis also demonstrated LC3-positive cytoplasmic puncta in TDP-43-depleted motor neurons, and the presence of these puncta was associated with shrinkage of motor neurons. This finding was confirmed by electron microscopy that revealed the presence of autolysosomes and autophagosomes in the motor neuronal cell bodies and axons of TDP CKO mice, suggesting that TDP-43 depletion resulted in dysregulation of the autophagic pathway. In addition, the accumulation of autophagic structures in the sciatic nerve and the disruption of retrograde labelling in TDP-43-lacking motor neurons suggest that the disruption of retrograde axonal transport may underlie the motor neuronal dysfunction in TDP CKO mice. Although the disruption of constitutive autophagy is shown to instigate the degeneration of certain types of neurons (Komatsu *et al.*, 2006), the causative role of the autophagic dysregulation in the pathogenesis of motor neuron diseases remains controversial. A recent work

demonstrates that motor neuron-specific knockout of the proteasome subunit Rpt3, but not autophagy mediator Atg7, leads to motor neuron degeneration in mice (Tashiro *et al.*, 2012), suggesting that the disruption of autophagic pathway in motor neurons may not be the primary cause of the neurodegeneration. However, accumulation of autophagosomes and autolysosomes was observed in the motor neurons of mice with mutant SOD1 (Li *et al.*, 2008; Tian *et al.*, 2011) and patients with sporadic ALS (Nakano *et al.*, 1993; Sasaki, 2011). In addition, mice carrying mutations of dynein or dynactin exhibit motor dysfunction with accumulation of autophagosomes in the motor neurons (Ravikumar *et al.*, 2005; Laird *et al.*, 2008). These lines of evidence may suggest a possible link between the increased autophagosomes and the process of motor neuron degeneration (Pasquali *et al.*, 2009; Chen *et al.*, 2012), although it remains unclear whether the accumulation of autophagosomes in neurodegenerative diseases results from activation of autophagy, disruption of retrograde transport or decreased lysosome fusion (Shintani and Klionsky, 2004; Baehrecke, 2005; Perlson *et al.*, 2010). Further investigation with regard to the linkage among loss of TDP-43, retrograde axonal transport and dysregulation of autophagy might contribute to our understanding the pathogenesis of ALS.

In conclusion, TDP CKO mice exhibited age-dependent motor impairment and morphological alterations in the motor neuron system that recapitulate several features of sporadic ALS neuropathology, including the accumulation of autophagosomes. These findings suggest that TDP-43 plays an essential role in the long-term maintenance of motor neurons, and that loss of TDP-43 function contributes to the pathogenesis of ALS.

Funding

This work was supported by a Centre of Excellence (COE) grant, a Grant in Aid for Scientific Research on Innovated Areas 'Foundation of Synapse and Neurocircuit Pathology', and Grants in-Aid from Ministry of Education, Culture, Sports, Science, and Technology (MEXT) of Japan; grants from the Ministry of Health, Labour and Welfare of Japan; and Core Research for Evolutional Science and Technology (CREST) of the Japan Science and Technology Agency (JST); Strategic Research Program for Brain Sciences of the MEXT of Japan.

Supplementary material

Supplementary material is available at *Brain* online.

References

Alexianu ME, Ho BK, Mohamed AH, La Bella V, Smith RG, Appel SH. The role of calcium-binding proteins in selective motoneuron vulnerability in amyotrophic lateral sclerosis. Ann Neurol 1994; 36: 846–58.

Arai T, Hasegawa M, Akiyama H, Ikeda K, Nonaka T, Mori H, et al. TDP-43 is a component of ubiquitin-positive tau-negative inclusions in frontotemporal lobar degeneration and amyotrophic lateral sclerosis. Biochem Biophys Res Commun 2006; 351: 602–11.

Arber S, Han B, Mendelsohn M, Smith M, Jessell TM, Sockanathan S. Requirement for the homeobox gene Hb9 in the consolidation of motor neuron identity. Neuron 1999; 23: 659–74.

Ayala YM, Misteli T, Baralle FE. TDP-43 regulates retinoblastoma protein phosphorylation through the repression of cyclin-dependent kinase 6 expression. Proc Natl Acad Sci USA 2008; 105: 3785–9.

Ayala YM, Pantano S, D'Ambrogio A, Buratti E, Brindisi A, Marchetti C, et al. Human, *Drosophila*, and *C.elegans* TDP43: nucleic acid binding properties and splicing regulatory function. J Mol Biol 2005; 348: 575–88.

Baehrecke EH. Autophagy: dual roles in life and death? Nat Rev Mol Cell Biol 2005; 6: 505–10.

Bradley WG, Good P, Rasool CG, Adelman LS. Morphometric and biochemical studies of peripheral nerves in amyotrophic lateral sclerosis. Ann Neurol 1983; 14: 267–77.

Buratti E, Brindisi A, Giombi M, Tisminetzky S, Ayala YM, Baralle FE. TDP-43 binds heterogeneous nuclear ribonucleoprotein A/B through its C-terminal tail: an important region for the inhibition of cystic fibrosis transmembrane conductance regulator exon 9 splicing. J Biol Chem 2005; 280: 37572–84.

Buratti E, De Conti L, Stuani C, Romano M, Baralle M, Baralle F. Nuclear factor TDP-43 can affect selected microRNA levels. FEBS J 2010; 277: 2268–81.

Chen S, Zhang X, Song L, Le W. Autophagy dysregulation in amyotrophic lateral sclerosis. Brain Pathol 2012; 22: 110–6.

Chiang PM, Ling J, Jeong YH, Price DL, Aja SM, Wong PC. Deletion of TDP-43 down-regulates Tbc1d1, a gene linked to obesity, and alters body fat metabolism. Proc Natl Acad Sci USA 2010; 107: 16320–4.

Feiguin F, Godena VK, Romano G, D'Ambrogio A, Klima R, Baralle FE. Depletion of TDP-43 affects *Drosophila* motoneurons terminal synapsis and locomotive behavior. FEBS Lett 2009; 583: 1586–92.

Fischer LR, Culver DG, Tennant P, Davis AA, Wang M, Castellano-Sanchez A, et al. Amyotrophic lateral sclerosis is a distal axonopathy: evidence in mice and man. Exp Neurol 2004; 185: 232–40.

Gitcho MA, Baloh RH, Chakraverty S, Mayo K, Norton JB, Levitch D, et al. TDP-43 A315T mutation in familial motor neuron disease. Ann Neurol 2008; 63: 535–8.

Igaz LM, Kwong LK, Lee EB, Chen-Plotkin A, Swanson E, Unger T, et al. Dysregulation of the ALS-associated gene TDP-43 leads to neuronal death and degeneration in mice. J Clin Invest 2011; 121: 726–38.

Iguchi Y, Katsuno M, Niwa J, Yamada S, Sone J, Waza M, et al. TDP-43 depletion induces neuronal cell damage through dysregulation of Rho family GTPases. J Biol Chem 2009; 284: 22059–66.

Kabashi E, Lin L, Tradewell ML, Dion PA, Bercier V, Bourgouin P, et al. Gain and loss of function of ALS-related mutations of TARDBP (TDP-43) cause motor deficits *in vivo*. Hum Mol Genet 2011; 19: 671–83.

Kabashi E, Valdmanis PN, Dion P, Spiegelman D, McConkey BJ, Vande Velde C, et al. TARDBP mutations in individuals with sporadic and familial amyotrophic lateral sclerosis. Nat Genet 2008; 40: 572–4.

Katsuno M, Adachi H, Kume A, Li M, Nakagomi Y, Niwa H, et al. Testosterone reduction prevents phenotypic expression in a transgenic mouse model of spinal and bulbar muscular atrophy. Neuron 2002; 35: 843–54.

Katsuno M, Adachi H, Minamiyama M, Waza M, Tokui K, Banno H, et al. Reversible disruption of dynactin 1-mediated retrograde axonal transport in polyglutamine-induced motor neuron degeneration. J Neurosci 2006; 26: 12106–17.

Komatsu M, Waguri S, Chiba T, Murata S, Iwata J, Tanida I, et al. Loss of autophagy in the central nervous system causes neurodegeneration in mice. Nature 2006; 441: 880–4.

Kraemer BC, Schuck T, Wheeler JM, Robinson LC, Trojanowski JQ, Lee VM, et al. Loss of murine TDP-43 disrupts motor function and plays an essential role in embryogenesis. Acta Neuropathol 2010; 119: 409–19.

Laird FM, Farah MH, Ackerley S, Hoke A, Maragakis N, Rothstein JD, et al. Motor neuron disease occurring in a mutant dynactin mouse

model is characterized by defects in vesicular trafficking. J Neurosci 2008; 28: 1997–2005.
Laslo P, Lipski J, Nicholson LF, Miles GB, Funk GD. Calcium binding proteins in motoneurons at low and high risk for degeneration in ALS. Neuroreport 2000; 11: 3305–8.
Lee EB, Lee VM, Trojanowski JQ. Gains or losses: molecular mechanisms of TDP43-mediated neurodegeneration. Nat Rev Neurosci 2011; 13: 38–50.
Li L, Zhang X, Le W. Altered macroautophagy in the spinal cord of SOD1 mutant mice. Autophagy 2008; 4: 290–3.
Misawa H, Nakata K, Toda K, Matsuura J, Oda Y, Inoue H, et al. VAChT-Cre. Fast and VAChT-Cre.Slow: postnatal expression of Cre recombinase in somatomotor neurons with different onset. Genesis 2003; 37: 44–50.
Nakano I, Shibata T, Uesaka Y. On the possibility of autolysosomal processing of skein-like inclusions. Electron microscopic observation in a case of amyotrophic lateral sclerosis. J Neurol Sci 1993; 120: 54–9.
Neumann M, Sampathu DM, Kwong LK, Truax AC, Micsenyi MC, Chou TT, et al. Ubiquitinated TDP-43 in frontotemporal lobar degeneration and amyotrophic lateral sclerosis. Science 2006; 314: 130–3.
Pasquali L, Longone P, Isidoro C, Ruggieri S, Paparelli A, Fornai F. Autophagy, lithium, and amyotrophic lateral sclerosis. Muscle Nerve 2009; 40: 173–94.
Perlson E, Maday S, Fu MM, Moughamian AJ, Holzbaur EL. Retrograde axonal transport: pathways to cell death? Trends Neurosci 2010; 33: 335–44.
Polymenidou M, Lagier-Tourenne C, Hutt KR, Huelga SC, Moran J, Liang TY, et al. Long pre-mRNA depletion and RNA missplicing contribute to neuronal vulnerability from loss of TDP-43. Nat Neurosci 2011; 14: 459–68.
Ravikumar B, Acevedo-Arozena A, Imarisio S, Berger Z, Vacher C, O'Kane CJ, et al. Dynein mutations impair autophagic clearance of aggregate-prone proteins. Nat Genet 2005; 37: 771–6.
Reiner A, Medina L, Figueredo-Cardenas G, Anfinson S. Brainstem motoneuron pools that are selectively resistant in amyotrophic lateral sclerosis are preferentially enriched in parvalbumin: evidence from monkey brainstem for a calcium-mediated mechanism in sporadic ALS. Exp Neurol 1995; 131: 239–50.
Sasaki S. Autophagy in spinal cord motor neurons in sporadic amyotrophic lateral sclerosis. J Neuropathol Exp Neurol 2011; 70: 349–59.
Sephton CF, Cenik C, Kucukural A, Dammer EB, Cenik B, Han Y, et al. Identification of neuronal RNA targets of TDP-43-containing ribonucleoprotein complexes. J Biol Chem 2011; 286: 1204–15.
Sephton CF, Good SK, Atkin S, Dewey CM, Mayer P III, Herz J, et al. TDP-43 is a developmentally regulated protein essential for early embryonic development. J Biol Chem 2010; 285: 6826–34.
Shan X, Chiang PM, Price DL, Wong PC. Altered distributions of Gemini of coiled bodies and mitochondria in motor neurons of TDP-43 transgenic mice. Proc Natl Acad Sci USA 2010; 107: 16325–30.
Shintani T, Klionsky DJ. Autophagy in health and disease: a double-edged sword. Science 2004; 306: 990–5.
Sreedharan J, Blair IP, Tripathi VB, Hu X, Vance C, Rogelj B, et al. TDP-43 mutations in familial and sporadic amyotrophic lateral sclerosis. Science 2008; 319: 1668–72.
Stallings NR, Puttaparthi K, Luther CM, Burns DK, Elliott JL. Progressive motor weakness in transgenic mice expressing human TDP-43. Neurobiol Dis 2010; 40: 404–14.
Strong MJ, Volkening K, Hammond R, Yang W, Strong W, Leystra-Lantz C, et al. TDP43 is a human low molecular weight neurofilament (hNFL) mRNA-binding protein. Mol Cell Neurosci 2007; 35: 320–7.
Swarup V, Phaneuf D, Bareil C, Robertson J, Rouleau GA, Kriz J, et al. Pathological hallmarks of amyotrophic lateral sclerosis/frontotemporal lobar degeneration in transgenic mice produced with TDP-43 genomic fragments. Brain 2011; 134: 2610–26.
Tashiro Y, Urushitani M, Inoue H, Koike M, Uchiyama Y, Komatsu M, et al. Motor neuron-specific disruption of proteasomes, but not autophagy, replicates amyotrophic lateral sclerosis. J Biol Chem 2012; 287: 42984–94.
Tian F, Morimoto N, Liu W, Ohta Y, Deguchi K, Miyazaki K, et al. *In vivo* optical imaging of motor neuron autophagy in a mouse model of amyotrophic lateral sclerosis. Autophagy 2011; 7: 985–92.
Tollervey JR, Curk T, Rogelj B, Briese M, Cereda M, Kayikci M, et al. Characterizing the RNA targets and position-dependent splicing regulation by TDP-43. Nat Neurosci 2011; 14: 452–8.
Tsai KJ, Yang CH, Fang YH, Cho KH, Chien WL, Wang WT, et al. Elevated expression of TDP-43 in the forebrain of mice is sufficient to cause neurological and pathological phenotypes mimicking FTLD-U. J Exp Med 2010; 207: 1661–73.
Uchida A, Sasaguri H, Kimura N, Tajiri M, Ohkubo T, Ono F, et al. Non-human primate model of amyotrophic lateral sclerosis with cytoplasmic mislocalization of TDP-43. Brain 2012; 135: 833–46.
Wang HY, Wang IF, Bose J, Shen CK. Structural diversity and functional implications of the eukaryotic TDP gene family. Genomics 2004; 83: 130–9.
Wegorzewska I, Bell S, Cairns NJ, Miller TM, Baloh RH. TDP-43 mutant transgenic mice develop features of ALS and frontotemporal lobar degeneration. Proc Natl Acad Sci USA 2009; 106: 18809–14.
Wils H, Kleinberger G, Janssens J, Pereson S, Joris G, Cuijt I, et al. TDP-43 transgenic mice develop spastic paralysis and neuronal inclusions characteristic of ALS and frontotemporal lobar degeneration. Proc Natl Acad Sci USA 2010; 107: 3858–63.
Wu LS, Cheng WC, Hou SC, Yan YT, Jiang ST, Shen CK. TDP-43, a neuro-pathosignature factor, is essential for early mouse embryogenesis. Genesis 2010; 48: 56–62.
Wu LS, Cheng WC, Shen CK. Targeted Depletion of TDP-43 Expression in the spinal cord motor neurons leads to the development of Amyotrophic Lateral Sclerosis (ALS)-like phenotypes in mice. J Biol Chem 2012; 287: 27335–44.
Xu YF, Gendron TF, Zhang YJ, Lin WL, D'Alton S, Sheng H, et al. Wild-type human TDP-43 expression causes TDP-43 phosphorylation, mitochondrial aggregation, motor deficits, and early mortality in transgenic mice. J Neurosci 2010; 30: 10851–9.
Yokoseki A, Shiga A, Tan CF, Tagawa A, Kaneko H, Koyama A, et al. TDP-43 mutation in familial amyotrophic lateral sclerosis. Ann Neurol 2008; 63: 538–42.
Zhang B, Tu P, Abtahian F, Trojanowski JQ, Lee VM. Neurofilaments and orthograde transport are reduced in ventral root axons of transgenic mice that express human SOD1 with a G93A mutation. J Cell Biol 1997; 139: 1307–15.
Zhou H, Huang C, Chen H, Wang D, Landel CP, Xia PY, et al. Transgenic rat model of neurodegeneration caused by mutation in the TDP gene. PLoS Genet 2010; 6: e1000887.

nature medicine

Naratriptan mitigates CGRP1-associated motor neuron degeneration caused by an expanded polyglutamine repeat tract

Makoto Minamiyama[1,3], Masahisa Katsuno[1,3], Hiroaki Adachi[1], Hideki Doi[1], Naohide Kondo[1], Madoka Iida[1], Shinsuke Ishigaki[1], Yusuke Fujioka[1], Shinjiro Matsumoto[1], Yu Miyazaki[1], Fumiaki Tanaka[1], Hiroki Kurihara[2] & Gen Sobue[1]

Spinal and bulbar muscular atrophy (SBMA) is a motor neuron disease caused by the expansion of the CAG triplet repeat within the androgen receptor (*AR*) gene. Here, we demonstrated that pathogenic AR upregulates the gene encoding calcitonin gene-related peptide α (CGRP1). In neuronal cells, overexpression of CGRP1 induced cellular damage via the activation of the c-Jun N-terminal kinase (JNK) pathway, whereas pharmacological suppression of CGRP1 or JNK attenuated the neurotoxic effects of pathogenic AR. The depletion of CGRP1 inactivated JNK and suppressed neurodegeneration in a mouse model of SBMA. Naratriptan, a serotonin 1B/1D (5-hydroxytryptamine 1B/1D, or 5-HT1B/1D) receptor agonist, decreased CGRP1 expression via the induction of dual-specificity protein phosphatase 1 (DUSP1), attenuated JNK activity and mitigated pathogenic AR-mediated neuronal damage in cellular and mouse SBMA models. These observations suggest that pharmacological activation of the 5-HT1B/1D receptor may be used therapeutically to treat SBMA and other polyglutamine-related neurodegenerative diseases.

The expansion of a genomic trinucleotide CAG repeat causes hereditary neurodegenerative disorders such as Huntington's disease, SBMA, dentatorubral-pallidoluysian atrophy and six forms of spinocerebellar ataxia[1,2]. SBMA, or Kennedy's disease, is a late-onset motor neuron disease characterized by progressive weakness and atrophy of bulbar, facial and limb muscles, which is attributable to the degeneration of lower motor neurons in the spinal cord and brainstem[3,4]. This disease is caused by an abnormal expansion of CAG repeats encoding the amino acid glutamine within the gene encoding AR, and it exclusively affects males carrying this type of mutation[5,6]. The pathogenic AR protein accumulates in the nucleus of motor neurons and causes several molecular changes, including transcriptional dysregulation, axonal transport defects, mitochondrial dysfunction and disruption of the transforming growth factor-β signaling pathway[7–17].

Dysregulation of the transcriptional machinery associated with histone hypoacetylation has been reported in cellular and animal models of polyglutamine diseases[18,19]. In addition to downregulation of genes that are necessary for the maintenance of normal cellular function, upregulation of certain molecules has also been observed in affected tissues in polyglutamine diseases[20,21]. These alterations of the normal gene expression profile seem to mediate polyglutamine toxicity in neuronal and non-neuronal cells and are partially reversed by histone acetylation[14,22,23]. However, it is unknown which genes are dysregulated and directly contribute to neurodegeneration.

Here, we performed a microarray analysis of the spinal cord of a mouse model of SBMA to identify the changes in gene expression that play a crucial part in polyglutamine-mediated neurodegeneration. We also examined whether genetic and pharmacological modulation of the expression of the identified genes could mitigate the histopathological and symptomatic effects of motor neuron degeneration.

RESULTS

Calcitonin gene–related peptide is upregulated in SBMA

To identify the gene expression changes that are specific to SBMA, we prepared total mRNA samples from the spinal cords of transgenic mice carrying a full-length human AR with 97 CAGs (AR-97Q), transgenic mice bearing a wild-type allele of AR with 24 CAGs (AR-24Q) and the wild-type littermates of the AR-97Q mice. Using microarray analysis, we identified genes with significantly altered expression among the three types of mice ($P < 0.005$). The expression of 124 genes were increased (>150%) or decreased (<67%) in male AR-97Q mice compared with their AR-24Q counterparts at the before-onset stage (7–9 weeks old). The expression of 12 of the 124 genes also showed a considerable difference between the AR-97Q and wild-type littermates but not between the AR-24Q and wild-type littermates (**Fig. 1a** and **Supplementary Table 1**). Among these candidates, we focused on the gene encoding calcitonin gene-related peptide 1 (Cgrp1) for the following reasons: (i) this gene, *Calca*, was

[1]Department of Neurology, Nagoya University Graduate School of Medicine, Nagoya, Japan. [2]Department of Physiological Chemistry and Metabolism, Graduate School of Medicine, University of Tokyo, Tokyo, Japan. [3]These authors contributed equally to this work. Correspondence should be addressed to M.K. (ka2no@med.nagoya-u.ac.jp) or G.S. (sobueg@med.nagoya-u.ac.jp).

Received 28 December 2011; accepted 13 August 2012; published online 30 September 2012; doi:10.1038/nm.2932

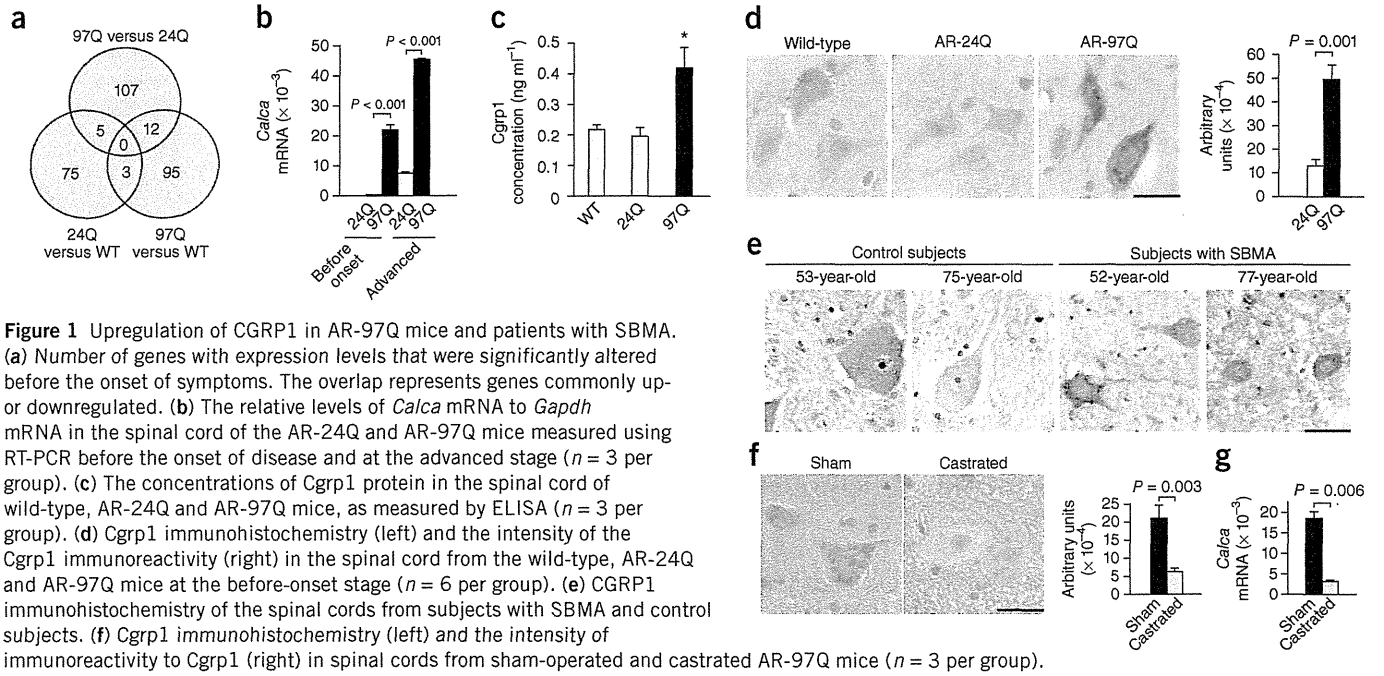

Figure 1 Upregulation of CGRP1 in AR-97Q mice and patients with SBMA. (**a**) Number of genes with expression levels that were significantly altered before the onset of symptoms. The overlap represents genes commonly up- or downregulated. (**b**) The relative levels of *Calca* mRNA to *Gapdh* mRNA in the spinal cord of the AR-24Q and AR-97Q mice measured using RT-PCR before the onset of disease and at the advanced stage ($n = 3$ per group). (**c**) The concentrations of Cgrp1 protein in the spinal cord of wild-type, AR-24Q and AR-97Q mice, as measured by ELISA ($n = 3$ per group). (**d**) Cgrp1 immunohistochemistry (left) and the intensity of the Cgrp1 immunoreactivity (right) in the spinal cord from the wild-type, AR-24Q and AR-97Q mice at the before-onset stage ($n = 6$ per group). (**e**) CGRP1 immunohistochemistry of the spinal cords from subjects with SBMA and control subjects. (**f**) Cgrp1 immunohistochemistry (left) and the intensity of immunoreactivity to Cgrp1 (right) in spinal cords from sham-operated and castrated AR-97Q mice ($n = 3$ per group). (**g**) The levels of *Calca* mRNA in spinal cords of sham-operated and castrated AR-97Q mice at the advanced stage ($n = 3$ per group). The scale bars indicate 20 μm (**d**,**e**) or 50 μm (**f**). The error bars indicate the s.e.m. $^*P < 0.05$ by analysis of variance (ANOVA) and Dunnett's test (**c**).

significantly upregulated in the AR-97Q mice compared with the other types of mice; (ii) the expression of this gene showed a further increase at the advanced stage (13–15 weeks old) (**Supplementary Table 1**); and (iii) this gene is expressed chiefly in lower motor neurons and dorsal root ganglion sensory neurons, not in glial or vascular endothelial cells[24]. We confirmed the results of the microarray using RT-PCR, which also showed strain- and stage-dependent upregulation of *Calca* mRNA (**Fig. 1b**).

The concentration of Cgrp1 in spinal cord tissue measured by ELISA was significantly higher in AR-97Q mice compared with AR-24Q or wild-type counterparts (**Fig. 1c**). Immunohistochemistry with Cgrp1-specific antibodies showed that Cgrp1 immunoreactivity

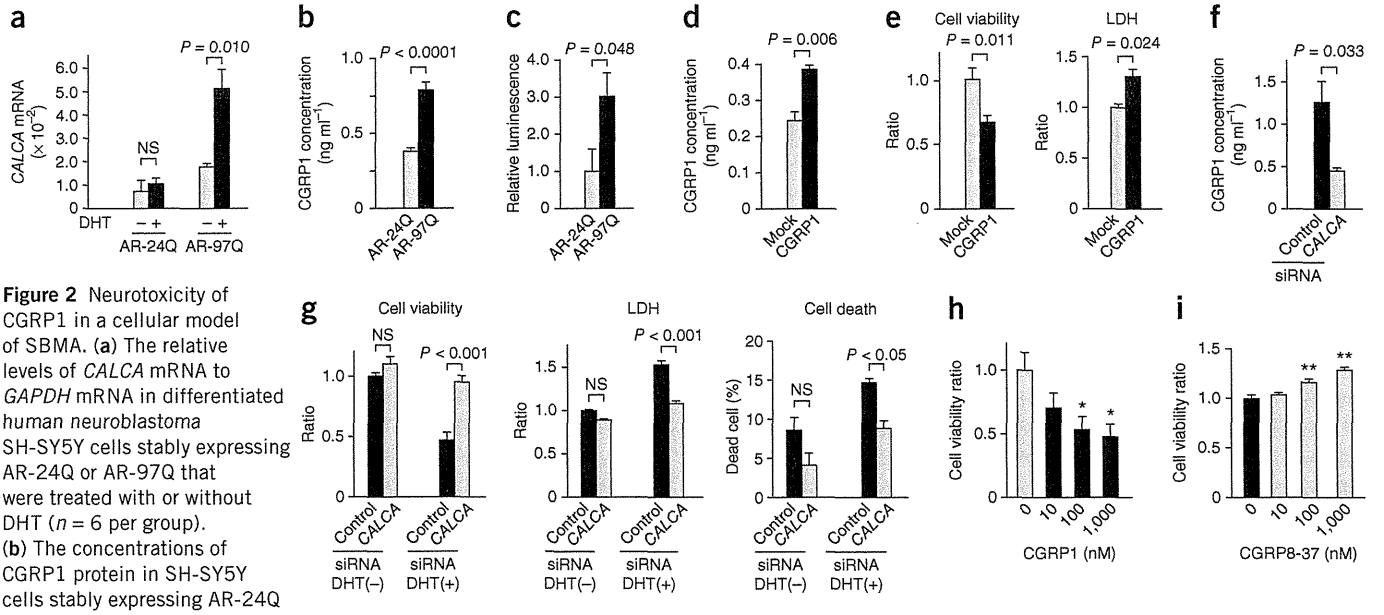

Figure 2 Neurotoxicity of CGRP1 in a cellular model of SBMA. (**a**) The relative levels of *CALCA* mRNA to *GAPDH* mRNA in differentiated human neuroblastoma SH-SY5Y cells stably expressing AR-24Q or AR-97Q that were treated with or without DHT ($n = 6$ per group). (**b**) The concentrations of CGRP1 protein in SH-SY5Y cells stably expressing AR-24Q or AR-97Q. (**c**) Luciferase activity transcriptionally regulated by the *CALCA* promoter in SH-SY5Y cells stably expressing AR-24Q or AR-97Q ($n = 6$ per group). (**d**) The concentrations of CGRP1 protein in SH-SY5Y cells transfected with a mock or CGRP1 vector ($n = 3$). (**e**) The viability as measured by cell viability WST-1 assay (left) and LDH release (right) of SH-SY5Y cells transfected with mock or CGRP1 vector ($n = 6$ per group). (**f**) The levels of CGRP1 protein in SH-SY5Y cells stably expressing AR-97Q transfected with control or *CALCA* siRNA ($n = 3$ per group). (**g**) The viability, LDH release and cell death (measured by Trypan blue dye exclusion) of SH-SY5Y cells stably expressing AR-97Q that were transfected with control or *CALCA* siRNA and treated with or without DHT ($n = 6$ per group). (**h**) The viability of SH-SY5Y cells treated with or without synthetic CGRP1 ($n = 6$ per group). (**i**) The viability of SH-SY5Y cells stably expressing AR-97Q treated with or without CGRP8-37, a CGRP1 receptor antagonist ($n = 6$ per group). $^*P < 0.05$ and $^{**}P < 0.01$ by ANOVA with Dunnett's test (**h**,**i**). The error bars indicate the s.e.m. NS, not significant.

in the spinal motor neurons was significantly stronger in the AR-97Q mice at both the before-onset and advanced stages (**Fig. 1d** and **Supplementary Fig. 1a,b**). Although we also detected Cgrp1 in the spinal dorsal horn, the expression of Cgrp1 was not different among the AR-97Q, AR-24Q and wild-type mice (data not shown). Cgrp1 is also expressed in other regions of the central nervous system, although the expression levels in these tissues are much lower than in the spinal cord (**Supplementary Fig. 2a**). Besides the spinal motor neurons, hypoglossal motor neurons and cerebellar granular cells also had high expression of Cgrp1, which accumulated in the cytoplasm of neurons with nuclear accumulation of the pathogenic AR (**Supplementary Fig. 2b,c**). Moreover, immunohistochemical analysis of autopsied human specimens showed higher expression of CGRP1 in the spinal motor neurons of subjects with SBMA compared to controls (**Fig. 1e** and **Supplementary Fig. 3a,b**). Because surgical or pharmacological suppression of testosterone release ameliorates the symptomatic and neuropathological changes in male AR-97Q mice[11,25], we examined the effects of the male sex hormone on the expression of CGRP1 in the mice. Surgical castration significantly decreased the immunoreactivity of Cgrp1 in the male AR-97Q mice (**Fig. 1f**), which is consistent with prior reports demonstrating the expression of CGRP1 is negatively regulated by testosterone[26]. The mRNA levels of *Calca* also decreased as a result of the castration (**Fig. 1g**).

CGRP1 mediates polyglutamine-dependent cytotoxicity

We further investigated the role of CGRP1 in polyglutamine-mediated neurotoxicity in differentiated human neuroblastoma SH-SY5Y cells stably expressing human AR containing 24 or 97 glutamines (AR-24Q and AR-97Q). In this cellular model, polyglutamine-expanded AR induced neurotoxicity and cell death in a testosterone-dependent manner (**Supplementary Fig. 4a–f**). In agreement with the data from the mouse model, cells expressing AR-97Q that were treated with dihydrotestosterone (DHT) had higher levels of *CALCA* mRNA than those bearing AR-24Q (**Fig. 2a**). SH-SY5Y cells expressing the pathogenic AR had higher protein amounts of CGRP1 and luciferase activity under control of the *CALCA* promoter (**Fig. 2b,c**).

We next investigated the relationship between expression of CGRP1 and viability of neuronal cells. Transient overexpression of CGRP1 in SH-SY5Y cells reduced viability and increased cellular damage as measured by the lactate dehydrogenase (LDH) assay (**Fig. 2d,e**). In contrast, siRNA-mediated knockdown of *CALCA* expression diminished the damage and death of cells stably expressing AR-97Q that were treated with DHT (**Fig. 2f,g**). CGRP1 is secreted from neurons, binds its receptors on the cell surface and functions as an autocrine and paracrine factor[27]. We thus examined the effect of CGRP1 on cellular viability via stimulation of its receptor. Administration of synthetic CGRP1 peptides dose-dependently decreased the viability of SH-SY5Y cells (**Fig. 2h**). In contrast, treatment with CGRP8-37, which is an antagonist of the CGRP receptor, attenuated the cytotoxicity caused by the pathogenic AR (**Fig. 2i**).

To confirm the result obtained in SH-SY5Y cell line, we examined the levels of Cgrp1 in mouse primary motor neurons infected with lentiviral vectors containing an N-terminal fragment of human AR with 24 or 97 glutamines (AR-24Q and AR-97Q)[17]. The pathogenic AR formed aggregates (**Supplementary Fig. 5a**) and increased the

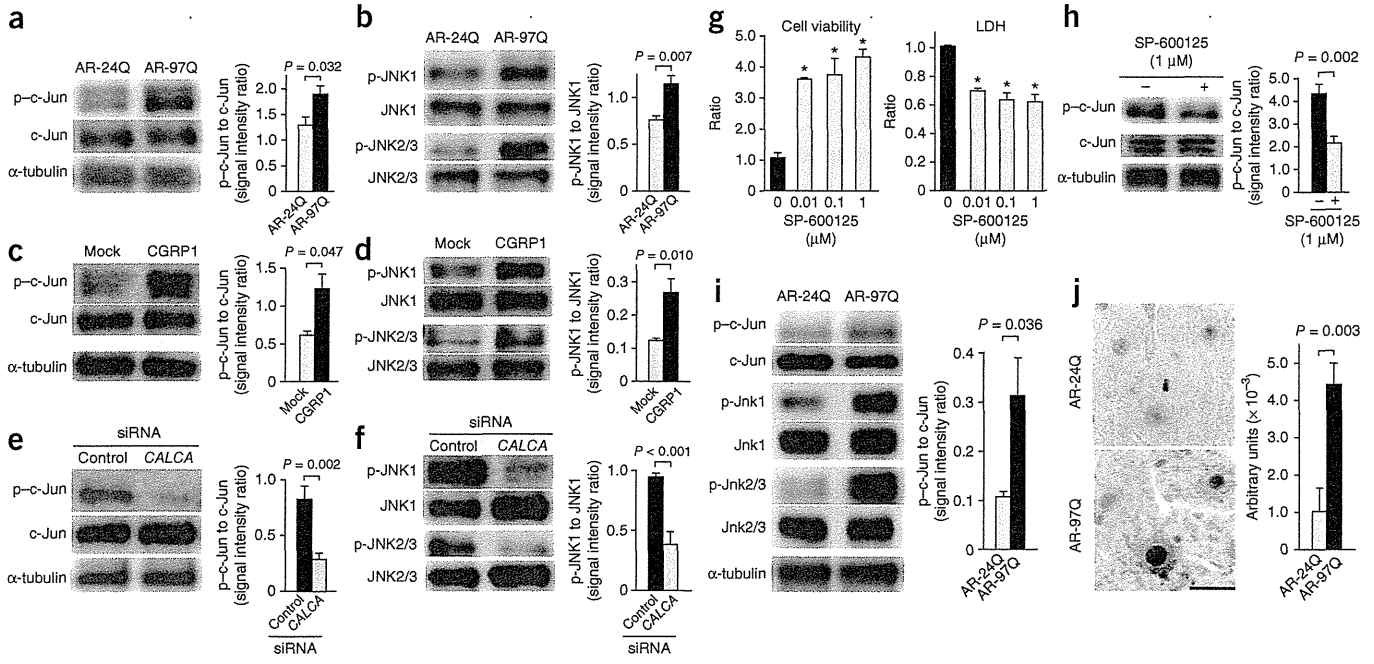

Figure 3 CGRP1 induces neuronal cell damage via activation of the JNK pathway. (**a**,**b**) Immunoblots for c-Jun (**a**) and JNK (**b**) and the relative intensities of immunoreactive bands from SH-SY5Y cells stably expressing AR-24Q and AR-97Q ($n = 6$ per group). (**c**,**d**) Immunoblots for c-Jun (**c**) and JNK (**d**) and the relative intensities of immunoreactive bands from SH-SY5Y cells transfected with the mock or CGRP1 vector ($n = 6$ per group). (**e**,**f**) Immunoblots for c-Jun (**e**) and JNK (**f**) and the relative intensities of immunoreactive bands from SH-SY5Y cells stably expressing AR-97Q transfected with control and *CALCA* siRNA ($n = 6$ per group). (**g**) The viability of (left) and LDH release from (right) SH-SY5Y cells stably expressing AR-97Q treated with a JNK inhibitor, SP-600125 ($n = 6$ per group). (**h**) Immunoblots and relative intensities of p–c-Jun immunoreactive bands from SH-SY5Y cells stably expressing AR-97Q and treated with SP-600125 ($n = 6$ per group). (**i**) Immunoblots (left) and the relative signal intensities (right) of the p–c-Jun immunoreactive bands for spinal cords from the AR-24Q and AR-97Q mice ($n = 6$ per group). (**j**) p–c-Jun immunohistochemistry (left) and the intensity of immunoreactivity to p–c-Jun (right) in spinal motor neurons of AR-24Q and AR-97Q mice ($n = 6$ per group). The scale bar indicates 20 μm. The error bars indicate the s.e.m. $^*P < 0.01$ by ANOVA with Dunnett's test (**g**).

mRNA levels of *Calca* in motor neurons (**Supplementary Fig. 5b**). Furthermore, administration of CGRP1 peptides decreased the viability of primary motor neurons (**Supplementary Fig. 5c**).

CGRP1 induces toxicity via the activation of c-Jun

CGRP1 is known to regulate various cellular signaling pathways, such as nuclear factor-κB (NF-κB) and JNK[28]. We next investigated the molecular mechanism by which CGRP1 elicited neuronal damage (**Supplementary Note** and **Supplementary Fig. 6a–c**). We found that AR-97Q increases the phosphorylation of c-Jun and JNK in neuronal cells treated with DHT (**Fig. 3a,b** and **Supplementary Figs. 7** and **8a**). We also observed activation of the JNK pathway by pathogenic AR in primary motor neurons (**Supplementary Fig. 8b**). Overexpression of CGRP1 also enhanced activation of the JNK pathway in SH-SY5Y cells (**Fig. 3c,d** and **Supplementary Fig. 7b,f**).

To determine whether pathogenic AR stimulates the JNK pathway via the upregulation of CGRP1, we knocked down expression of *CALCA* using siRNA in SH-SY5Y cells stably expressing AR-97Q that are treated with DHT. Transfection of *CALCA* siRNA suppressed activation of the JNK pathway (**Fig. 3e,f** and **Supplementary Fig. 7c,g**). Furthermore, pharmacological inhibition of JNK by SP-600125 increased cell viability and suppressed cytotoxic damage in SH-SY5Y cells stably expressing AR-97Q (**Fig. 3g,h**) and in those treated with CGRP1 peptides (**Supplementary Fig. 8c**). Immunoblot and histopathological analyses also demonstrated activation of the JNK pathway in the AR-97Q mice (**Fig. 3i,j** and **Supplementary Fig. 7d**).

Calca depletion ameliorates motor neuron degeneration

To clarify the role of CGRP1 in the pathogenic processes of SBMA, we next investigated the biological effects of depletion of *Calca* in male AR-97Q mice. Homozygous deletion of the *Calca* gene improved motor function, as assessed by the rotarod task and grip strength, increased body weight and extended the lifespan of the AR-97Q *Calca*$^{-/-}$ mice (**Fig. 4a**). We confirmed that the Cgrp1 protein was depleted in the spinal motor neurons of male AR-97Q *Calca*$^{-/-}$ mice (**Fig. 4b,c**). Histopathological analyses of the skeletal muscles showed that neurogenic amyotrophy was attenuated by depletion of *Calca* (**Fig. 4d**).

Depletion of *Calca* mitigated reactive astrogliosis in the spinal cord of AR-97Q mice, as assessed by GFAP staining at the advanced stage (**Fig. 4e**). Depletion of *Calca* also upregulated the expression of choline acetyltransferase (ChAT), a marker of motor neuronal function (**Fig. 4f,g**). We confirmed that *Calca* depletion had no detectable effects on motor function or ChAT expression in wild-type mice (**Supplementary Fig. 9a–h**). In addition, histopathological and immunoblot analyses showed that deletion of the *Calca* gene suppressed the phosphorylation of c-Jun in the spinal motor neurons of male AR-97Q mice (**Fig. 4h** and **Supplementary Fig. 9i**).

CGRP1 suppression mitigates polyglutamine toxicity

CGRP1 has been implicated in the molecular pathogenesis of migraines, and 5-HT1B/1D receptor agonists have been shown to suppress the expression and secretion of CGRP1 in neurons[29]. We thus determined whether these antimigraine drugs could alleviate polyglutamine-mediated neurotoxicity by decreasing the expression of CGRP1 in neuronal cells. The 5-HT1B/1D receptor agonists sumatriptan, naratriptan and rizatriptan reduced the cellular damage and restored the viability of SH-SY5Y cells that stably expressed AR-97Q (**Fig. 5a**). Given that naratriptan has the longest half-life among these drugs, it may be an appropriate candidate for the treatment

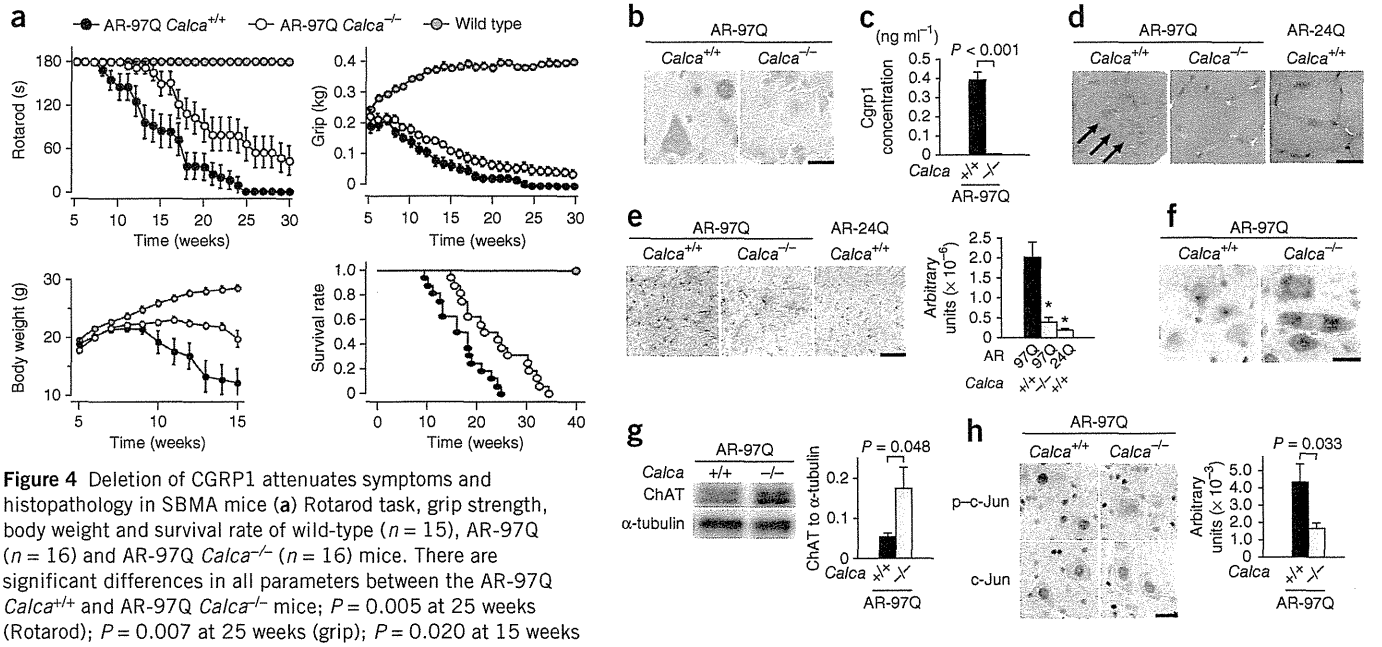

Figure 4 Deletion of CGRP1 attenuates symptoms and histopathology in SBMA mice (**a**) Rotarod task, grip strength, body weight and survival rate of wild-type ($n = 15$), AR-97Q ($n = 16$) and AR-97Q *Calca*$^{-/-}$ ($n = 16$) mice. There are significant differences in all parameters between the AR-97Q *Calca*$^{+/+}$ and AR-97Q *Calca*$^{-/-}$ mice; $P = 0.005$ at 25 weeks (Rotarod); $P = 0.007$ at 25 weeks (grip); $P = 0.020$ at 15 weeks (body weight); and $P = 0.003$ (survival). (**b**) Cgrp1 immunohistochemistry of spinal cords from AR-97Q *Calca*$^{+/+}$ and AR-97Q *Calca*$^{-/-}$ mice (15 weeks old). (**c**) The concentrations of Cgrp1 protein in the spinal cord of AR-97Q *Calca*$^{+/+}$ and AR-97Q *Calca*$^{-/-}$ mice as measured by ELISA ($n = 3$ per group). (**d**) H&E staining of skeletal muscle from AR-97Q *Calca*$^{+/+}$, AR-97Q *Calca*$^{-/-}$ and AR-24Q mice. (**e**) Gfap immunohistochemistry (left) and intensity of immunoreactivity to Gfap (right) in spinal cord sections from AR-97Q *Calca*$^{+/+}$, AR-97Q *Calca*$^{-/-}$ and AR-24Q mice ($n = 6$ per group). (**f**) ChAT immunohistochemistry in spinal cord sections from AR-97Q *Calca*$^{+/+}$ and AR-97Q *Calca*$^{-/-}$ mice. (**g**) Immunoblots (left) and relative signal intensities of ChAT-immunoreactive bands (right) of spinal cords from the AR-97Q *Calca*$^{+/+}$ and AR-97Q *Calca*$^{-/-}$ mice ($n = 6$ per group). (**h**) c-Jun immunohistochemistry (left) and intensity of immunoreactivity to p–c-Jun (right) in spinal cords from AR-97Q *Calca*$^{+/+}$ and AR-97Q *Calca*$^{-/-}$ mice ($n = 6$ per group). The scale bars indicate 20 μm (**b**,**f**,**h**) or 50 μm (**d**,**e**). The error bars indicate the s.e.m. $^*P < 0.01$ by ANOVA with Dunnett's test (**e**).

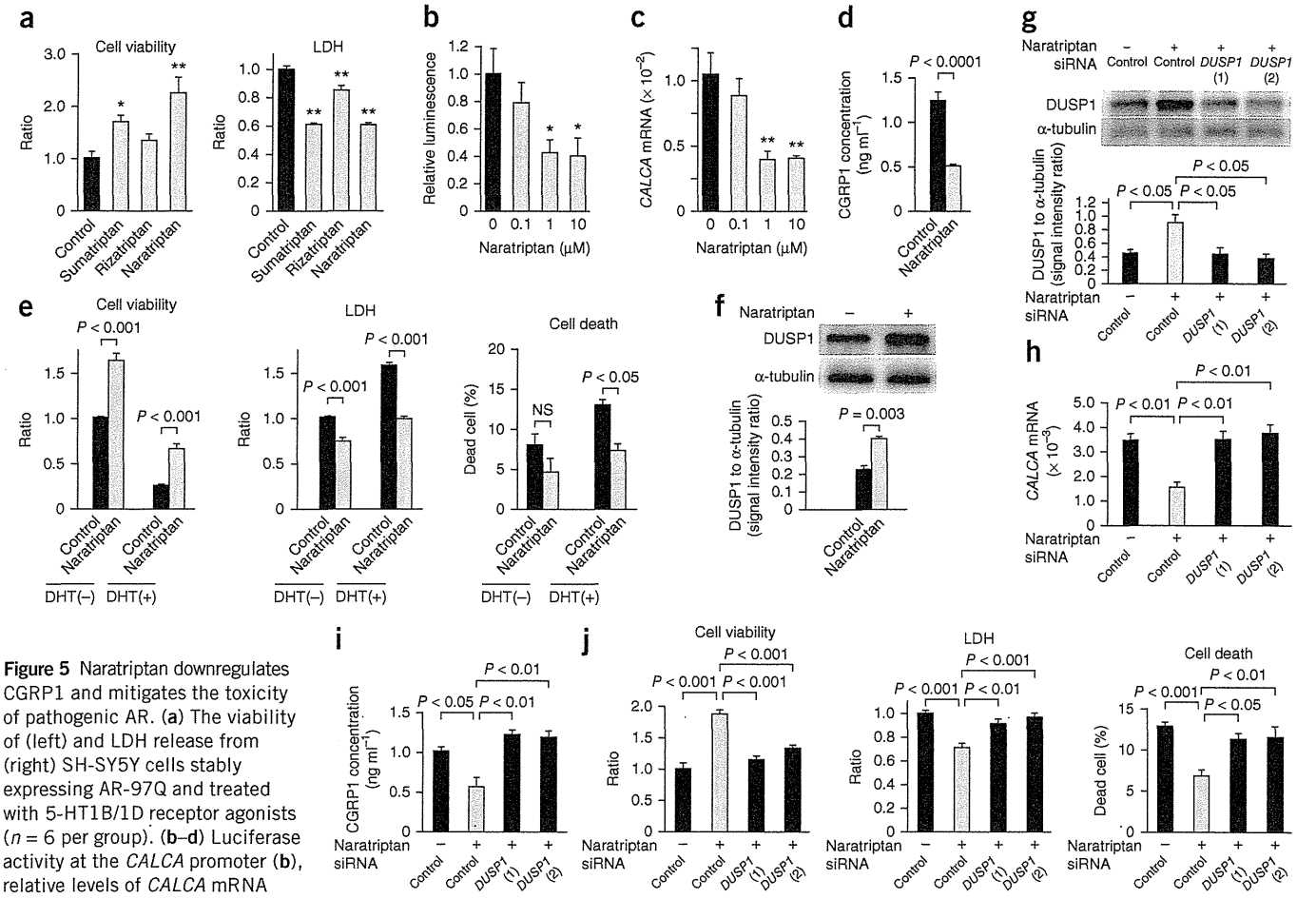

Figure 5 Naratriptan downregulates CGRP1 and mitigates the toxicity of pathogenic AR. (**a**) The viability of (left) and LDH release from (right) SH-SY5Y cells stably expressing AR-97Q and treated with 5-HT1B/1D receptor agonists ($n = 6$ per group). (**b–d**) Luciferase activity at the *CALCA* promoter (**b**), relative levels of *CALCA* mRNA relative to *GAPDH* mRNA (**c**) and concentration of CGRP1 (**d**) in SH-SY5Y cells that stably express AR-97Q and were treated with naratriptan ($n = 6$ per group). (**e**) The viability, LDH release and cell death of SH-SY5Y cells stably expressing AR-97Q that were treated with naratriptan and DHT ($n = 6$ per group). (**f**) Immunoblots (top) and relative signal intensities of DUSP1-immunoreactive bands (bottom) of SH-SY5Y cells stably expressing AR-97Q that were treated with or without naratriptan ($n = 3$ per group). (**g**) Immunoblots (top) and relative signal intensities of DUSP1-immunoreactive bands (bottom) of SH-SY5Y cells stably expressing AR-97Q that were transfected with the control or *DUSP1* siRNA and treated with or without naratriptan ($n = 3$ per group). (**h,i**) Relative levels of *CALCA* mRNA to *GAPDH* mRNA (**h**) and CRGP1 protein concentration (**i**) in SH-SY5Y cells stably expressing AR-97Q that were transfected with control or *DUSP1* siRNA and treated with naratriptan ($n = 3$ per group). (**j**) Viability, LDH release and cell death of SH-SY5Y cells stably expressing AR-97Q that were transfected with control or *DUSP1* siRNA and treated with naratriptan ($n = 6$ per group). The error bars indicate the s.e.m. $^*P < 0.05$ and $^{**}P < 0.01$ by ANOVA with Dunnett's test (**a–c**). Statistical analysis was performed using ANOVA with Tukey's test (**g–j**). NS, not significant.

of SBMA[30]. Therefore, we investigated the effects of naratriptan on the expression of CGRP1 and on polyglutamine-mediated cytotoxicity in neuronal cells. Administration of naratriptan reduced luciferase activity under control of the *CALCA* promoter as well as the mRNA and protein levels of CGRP1 in SH-SY5Y cells stably expressing AR-97Q (**Fig. 5b–d**). Naratriptan restored cell viability and suppressed the release of LDH, which is a marker of cytotoxicity, in cells treated with or without DHT, although the effects were more pronounced in the presence of DHT (**Fig. 5e**). Moreover, the effects of naratriptan on cell death were observable only when the SH-SY5Y cells expressing AR-97Q were treated with DHT (**Fig. 5e**).

Previous studies have suggested that 5-HT1B/1D receptor agonists suppress the expression of CGRP1 via the induction of DUSP1, a suppressor of the mitogen-activated protein kinase pathway[31]. We thus examined whether the neuroprotective effects of naratriptan are mediated by DUSP1. Naratriptan increased the expression of DUSP1 (**Fig. 5f**). SiRNA-mediated knockdown of *DUSP1* attenuated the effects of naratriptan on CGRP1 expression and neuroprotection in SH-SY5Y cells expressing AR-97Q (**Fig. 5g–j**). Pharmacological inhibition of DUSP1 with Ro-31-8220 in SH-SY5Y cells and primary motor neurons also attenuated naratriptan-mediated neuroprotection (**Supplementary Fig. 10a–g**). Furthermore, pharmacological inhibition of the 5-HT1B/1D receptor also inhibited the effects of naratriptan on CGRP1 expression and neuroprotection (**Supplementary Fig. 11a,b**), confirming that this receptor is involved in naratriptan-mediated suppression of the toxicity of the pathogenic AR.

We next investigated the effects of pharmacological stimulation of the 5-HT1B/1D receptor in a mouse model of SBMA. Oral administration of naratriptan improved grip strength and performance in the rotarod task of male AR-97Q mice in a dose-dependent manner as compared to vehicle-treated control AR-97Q mice (**Fig. 6a**). This pharmacological intervention also increased body weight and lifespan, although it showed no detectable effects on these phenotypes in wild-type mice (**Fig. 6a** and **Supplementary Fig. 12**). In agreement with the results of the cellular experiments, expression

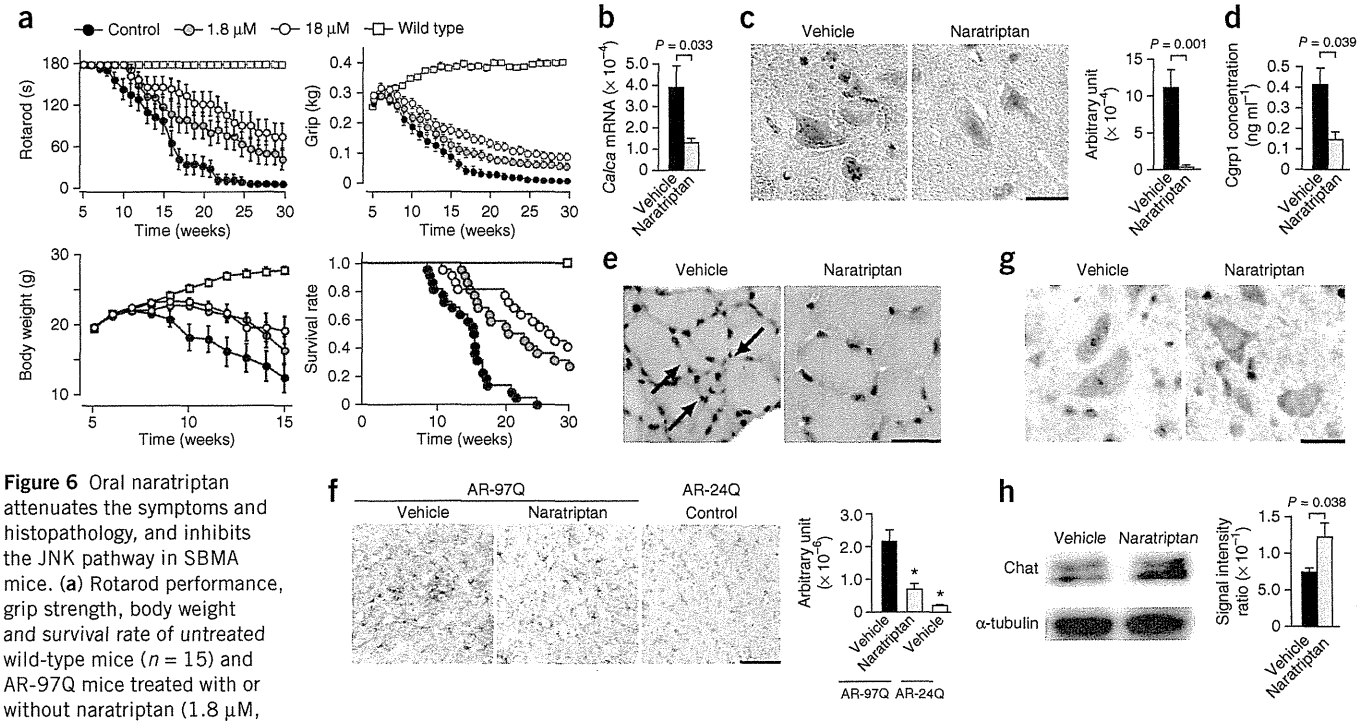

Figure 6 Oral naratriptan attenuates the symptoms and histopathology, and inhibits the JNK pathway in SBMA mice. (**a**) Rotarod performance, grip strength, body weight and survival rate of untreated wild-type mice ($n = 15$) and AR-97Q mice treated with or without naratriptan (1.8 μM, $n = 22$; 18 μM, $n = 22$). Significant differences were observed in all parameters between the untreated ($n = 22$) and 18 μM naratriptan–treated AR-97Q mice: $P < 0.01$ at 25 weeks (rotarod); $P < 0.01$ at 25 weeks (grip); $P < 0.05$ at 15 weeks (body weight); and $P < 0.0001$ (survival). (**b**) Relative levels of *Calca* mRNA to *Gapdh* mRNA in the spinal cords of AR-97Q mice treated with or without naratriptan ($n = 3$ per group). (**c**) Cgrp1 immunohistochemistry and intensity of immunoreactivity to Cgrp1 in spinal cords from AR-97Q mice treated with or without naratriptan ($n = 6$ per group). (**d**) The concentrations of Cgrp1 protein in the spinal cord of AR-97Q mice treated with or without naratriptan ($n = 3$ per group). (**e**) H&E staining of skeletal muscle from AR-97Q mice treated with or without naratriptan. (**f**) Gfap immunohistochemistry (left) and intensity of immunoreactivity to Gfap (right) in spinal cord sections from AR-97Q mice treated with or without naratriptan ($n = 6$ per group). (**g**) ChAT immunohistochemistry in spinal cord sections from AR-97Q mice treated with or without naratriptan. (**h**) Immunoblots and relative intensities of ChAT-immunoreactive bands of spinal cords from AR-97Q mice treated with or without naratriptan ($n = 6$ per group). The scale bars indicate 20 μm (**c**,**g**) or 50 μm (**e**,**f**). The error bars indicate the s.e.m. $^*P < 0.01$ by ANOVA with Dunnett's test (**f**).

of *Calca* was lower in the spinal cords of male AR-97Q mice treated with naratriptan as compared to vehicle-treated controls (**Fig. 6b**). Immunohistochemistry and ELISA revealed that naratriptan suppressed expression of Cgrp1 at the protein level in the spinal motor neurons of SBMA mice (**Fig. 6c,d**). Histopathological analyses indicated that oral naratriptan also reduced muscle wasting, suppressed reactive astrogliosis and increased expression of ChAT in the spinal motor neurons of AR-97Q mice (**Fig. 6e–h**).

Naratriptan suppresses the JNK pathway

To elucidate the molecular basis for the neuroprotection induced by naratriptan, we investigated the effects of this drug on the activity of the JNK pathway. Naratriptan treatment decreased the phosphorylation of c-Jun in SH-SY5Y cells stably expressing AR-97Q and treated with DHT (**Supplementary Fig. 13a,b**). Immunoblotting and immunohistochemistry showed that oral naratriptan also reduced the phosphorylation of c-Jun in the spinal cords of male AR-97Q mice (**Supplementary Fig. 14a,b**). Since the activation of JNK by pathogenic AR disrupts axonal transport, which contributes to the pathogenesis of SBMA[17,32], we investigated the effects of naratriptan on axonal transport. Naratriptan increased the number of motor neurons labeled with FluoroGold, a tracer used to measure retrograde axonal transport in mice (**Supplementary Fig. 15a,b**). As for the safety of naratriptan, we did not observe any adverse effects of oral treatment with naratriptan at 18 μM for 8–10 weeks on liver or renal function (**Supplementary Fig. 15c**).

DISCUSSION

Here we showed that the pathogenic AR protein dysregulates transcription in a mouse model of SBMA before the onset of motor impairment. Among the disease-specific transcriptional changes, CGRP1 was upregulated as the disease progressed and was also found to be upregulated in humans with SBMA and in a cellular model of SBMA. Alterations of gene expression have been demonstrated by microarray analyses of human postmortem specimens and in cellular and animal models of polyglutamine diseases, suggesting that transcriptional dysregulation is central to the pathogenesis of polyglutamine diseases that is independent of the context of the causative protein[22,33,34]. We found that pathogenic AR proteins increase activity at the *CALCA* gene promoter, which indicates that the transcription of CGRP1 is upregulated by pathogenic AR in SBMA.

CGRP1 is known to be upregulated upon neuronal injury, which suggests a potential neuroprotective role of this molecule[35]. On the contrary, elevated expression of CGRP1 is reported to be correlated with increased vulnerability of motor neurons in a mouse model of amyotrophic lateral sclerosis linked to a mutation in the gene encoding superoxide dismutase 1 (SOD1)[36]. Depletion of *Calca*, however, has no effect on the disease progression in mutant *Sod1* mice, suggesting that the basal expression of CGRP1 has neither neurotoxic nor neuroprotective effects[37]. Alternatively, other molecules may overwhelm the effects of CGRP1 on motor neuron degeneration in amyotrophic lateral sclerosis. In contrast, our study shows that increased expression of CGRP1 reduces the viability and induces

damage of neuronal cells. Moreover, genetic suppression of the pathogenic AR–induced upregulation of CGRP1 mitigated neuronal damage in mice. Our findings thus indicate that increased expression of CGRP1 contributes to motor neuron degeneration in SBMA.

CGRP1 is a multifunctional neuropeptide that has a potent vasodilatory effect and is believed to have a key role in vascular headaches[24]. In the nervous system, CGRP1 is also known to regulate nociceptor activation, neuroinflammation and neuronal nicotinic receptor functions[38,39]. Our study shows that overexpression of CGRP1 induces cytotoxicity in neuronal cells, and deletion of *Calca* ameliorates motor neuron damage in the mouse model of SBMA. We also found that pathogenic AR activates the JNK pathway via upregulation of CGRP1 in cellular and mouse models of SBMA. In agreement with our results, CGRP1 was previously shown to activate the JNK pathway in neuroblastoma cells[40]. In addition, we have found that activation of the JNK pathway enhances neuronal damage and that pharmacological inhibition of JNK mitigates the toxicity of pathogenic AR in neuronal cells. Abnormal activation of the JNK pathway has also been implicated in the pathogenesis of neurodegenerative disorders, including SBMA[32,41–44].

On the basis of its potent effects on neuroinflammation, CGRP1 has been identified as a therapeutic target for migraines[45]. Agonists of the 5-HT1B/1D receptor, which are clinically used for the suppression of migraines, reduce the serum levels of CGRP1 (ref. 29). Here we showed that the antimigraine drug naratriptan and other 5-HT1B/1D receptor agonists reduce promoter activity of the gene encoding CGRP1 and decrease mRNA levels of *CALCA* in neuronal cells via the induction of DUSP1. Oral administration of naratriptan also decreased the expression of Cgrp1 and ameliorated the motor impairment in a mouse model of SBMA. Furthermore, our study also showed that naratriptan treatment inhibits the JNK pathway in cellular and mouse models of SBMA. These observations indicate that stimulation of the 5-HT1B/1D receptor suppresses the neurotoxicity of polyglutamine-expanded AR by downregulating CGRP1 resulting in inactivation of the JNK pathway. As naratriptan is widely used in patients with migraine, this drug is a potential candidate for SBMA therapy. However, the efficacy awaits further clinical trials in patients given the limited efficacy of androgen ablation trials, despite the complete suppression of neurodegeneration in AR-97Q mice by leuprorelin[25,46,47]. As naratriptan showed limited effects on survival and motor function in the SBMA model mice, further studies are needed to evaluate the efficacy and safety of long-term treatment with naratriptan in humans.

METHODS

Methods and any associated references are available in the online version of the paper.

Accession codes. Microarray data have been deposited in the Gene Expression Omnibus (GEO) with accession code GSE39865.

Note: Supplementary information is available in the online version of the paper.

ACKNOWLEDGMENTS

This work was supported by a Center-of-Excellence grant, a Grant-in-Aid for Scientific Research on Innovated Areas "Foundation of Synapse and Neurocircuit Pathology" (No. 22110005) and Grants-in-Aid from the Ministry of Education, Culture, Sports, Science and Technology, Japan (Nos. 21229011, 21689024 and 23390230); grants from the Ministry of Health, Labor and Welfare, Japan; Core Research for Evolutional Science and Technology (CREST) from Japan Science and Technology Agency (JST); and a grant from the Kennedy Disease Association.

AUTHOR CONTRIBUTIONS

Project planning was performed by M.M., M.K., H.K. and G.S.; microarray analysis by M.M. and M.K.; cellular analysis by M.M., M.K., H.A., H.D., S.M. and Y.M.; primary motor neuron culture by M.K., S.I. and Y.F.; animal work by M.M., M.K., N.K. and M.I.; tissue staining by M.M., M.K. and M.I.; and data analysis by M.M., M.K., F.T. and G.S. M.M. and M.K. drafted the manuscript, and F.T., H.K. and G.S. revised it critically for intellectual content.

COMPETING FINANCIAL INTERESTS

The authors declare no competing financial interests.

Published online at http://www.nature.com/doifinder/10.1038/nm.2932.
Reprints and permissions information is available online at http://www.nature.com/reprints/index.html.

1. Ross, C.A. & Tabrizi, S.J. Huntington's disease: from molecular pathogenesis to clinical treatment. *Lancet Neurol.* **10**, 83–98 (2011).
2. Gatchel, J.R. & Zoghbi, H.Y. Diseases of unstable repeat expansion: mechanisms and common principles. *Nat. Rev. Genet.* **6**, 743–755 (2005).
3. Finsterer, J. Perspectives of Kennedy's disease. *J. Neurol. Sci.* **298**, 1–10 (2010).
4. Katsuno, M. *et al.* Pathogenesis, animal models and therapeutics in spinal and bulbar muscular atrophy (SBMA). *Exp. Neurol.* **200**, 8–18 (2006).
5. La Spada, A.R., Wilson, E.M., Lubahn, D.B., Harding, A.E. & Fischbeck, K.H. Androgen receptor gene mutations in X-linked spinal and bulbar muscular atrophy. *Nature* **352**, 77–79 (1991).
6. Schmidt, B.J., Greenberg, C.R., Allingham-Hawkins, D.J. & Spriggs, E.L. Expression of X-linked bulbospinal muscular atrophy (Kennedy disease) in two homozygous women. *Neurology* **59**, 770–772 (2002).
7. Sobue, G. *et al.* X-linked recessive bulbospinal neuronopathy. A clinicopathological study. *Brain* **112**, 209–232 (1989).
8. Adachi, H. *et al.* Widespread nuclear and cytoplasmic accumulation of mutant androgen receptor in SBMA patients. *Brain* **128**, 659–670 (2005).
9. Bauer, P.O. & Nukina, N. The pathogenic mechanisms of polyglutamine diseases and current therapeutic strategies. *J. Neurochem.* **110**, 1737–1765 (2009).
10. Shao, J. & Diamond, M.I. Polyglutamine diseases: emerging concepts in pathogenesis and therapy. *Hum. Mol. Genet.* **16 Spec No. 2**, R115–R123 (2007).
11. Katsuno, M. *et al.* Testosterone reduction prevents phenotypic expression in a transgenic mouse model of spinal and bulbar muscular atrophy. *Neuron* **35**, 843–854 (2002).
12. Takeyama, K. *et al.* Androgen-dependent neurodegeneration by polyglutamine-expanded human androgen receptor in *Drosophila*. *Neuron* **35**, 855–864 (2002).
13. Nedelsky, N.B. *et al.* Native functions of the androgen receptor are essential to pathogenesis in a *Drosophila* model of spinobulbar muscular atrophy. *Neuron* **67**, 936–952 (2010).
14. Minamiyama, M. *et al.* Sodium butyrate ameliorates phenotypic expression in a transgenic mouse model of spinal and bulbar muscular atrophy. *Hum. Mol. Genet.* **13**, 1183–1192 (2004).
15. Katsuno, M. *et al.* Reversible disruption of dynactin 1–mediated retrograde axonal transport in polyglutamine-induced motor neuron degeneration. *J. Neurosci.* **26**, 12106–12117 (2006).
16. Ranganathan, S. *et al.* Mitochondrial abnormalities in spinal and bulbar muscular atrophy. *Hum. Mol. Genet.* **18**, 27–42 (2009).
17. Katsuno, M. *et al.* Disrupted transforming growth factor-β signaling in spinal and bulbar muscular atrophy. *J. Neurosci.* **30**, 5702–5712 (2010).
18. Steffan, J.S. *et al.* Histone deacetylase inhibitors arrest polyglutamine-dependent neurodegeneration in *Drosophila*. *Nature* **413**, 739–743 (2001).
19. Butler, R. & Bates, G.P. Histone deacetylase inhibitors as therapeutics for polyglutamine disorders. *Nat. Rev. Neurosci.* **7**, 784–796 (2006).
20. Luthi-Carter, R. *et al.* Decreased expression of striatal signaling genes in a mouse model of Huntington's disease. *Hum. Mol. Genet.* **9**, 1259–1271 (2000).
21. Obrietan, K. & Hoyt, K.R. CRE-mediated transcription is increased in Huntington's disease transgenic mice. *J. Neurosci.* **24**, 791–796 (2004).
22. Sugars, K.L. & Rubinsztein, D.C. Transcriptional abnormalities in Huntington disease. *Trends Genet.* **19**, 233–238 (2003).
23. Mo, K. *et al.* Microarray analysis of gene expression by skeletal muscle of three mouse models of Kennedy disease/spinal bulbar muscular atrophy. *PLoS ONE* **5**, e12922 (2010).
24. Ho, T.W., Edvinsson, L. & Goadsby, P.J. CGRP and its receptors provide new insights into migraine pathophysiology. *Nat. Rev. Neurol.* **6**, 573–582 (2010).
25. Katsuno, M. *et al.* Leuprorelin rescues polyglutamine-dependent phenotypes in a transgenic mouse model of spinal and bulbar muscular atrophy. *Nat. Med.* **9**, 768–773 (2003).
26. Popper, P. & Micevych, P.E. The effect of castration on calcitonin gene–related peptide in spinal motor neurons. *Neuroendocrinology* **50**, 338–343 (1989).
27. Ma, W. *et al.* Localization and modulation of calcitonin gene-related peptide-receptor component protein-immunoreactive cells in the rat central and peripheral nervous systems. *Neuroscience* **120**, 677–694 (2003).
28. Walker, C.S., Conner, A.C., Poyner, D.R. & Hay, D.L. Regulation of signal transduction by calcitonin gene–related peptide receptors. *Trends Pharmacol. Sci.* **31**, 476–483 (2010).

29. Durham, P.L. & Russo, A.F. New insights into the molecular actions of serotonergic antimigraine drugs. *Pharmacol. Ther.* **94**, 77–92 (2002).
30. Jhee, S.S., Shiovitz, T., Crawford, A.W. & Cutler, N.R. Pharmacokinetics and pharmacodynamics of the triptan antimigraine agents: a comparative review. *Clin. Pharmacokinet.* **40**, 189–205 (2001).
31. Durham, P.L. & Russo, A.F. Serotonergic repression of mitogen-activated protein kinase control of the calcitonin gene–related peptide enhancer. *Mol. Endocrinol.* **12**, 1002–1009 (1998).
32. Morfini, G. *et al.* JNK mediates pathogenic effects of polyglutamine-expanded androgen receptor on fast axonal transport. *Nat. Neurosci.* **9**, 907–916 (2006).
33. Serra, H.G. *et al.* Gene profiling links SCA1 pathophysiology to glutamate signaling in Purkinje cells of transgenic mice. *Hum. Mol. Genet.* **13**, 2535–2543 (2004).
34. Becanovic, K. *et al.* Transcriptional changes in Huntington disease identified using genome-wide expression profiling and cross-platform analysis. *Hum. Mol. Genet.* **19**, 1438–1452 (2010).
35. Zheng, L.F. *et al.* Calcitonin gene–related peptide dynamics in rat dorsal root ganglia and spinal cord following different sciatic nerve injuries. *Brain Res.* **1187**, 20–32 (2008).
36. Ringer, C., Weihe, E. & Schutz, B. Calcitonin gene–related peptide expression levels predict motor neuron vulnerability in the superoxide dismutase 1-G93A mouse model of amyotrophic lateral sclerosis. *Neurobiol. Dis.* **45**, 547–554 (2012).
37. Ringer, C., Weihe, E. & Schutz, B. Pre-symptomatic alterations in subcellular betaCGRP distribution in motor neurons precede astrogliosis in ALS mice. *Neurobiol. Dis.* **35**, 286–295 (2009).
38. Di Angelantonio, S., Giniatullin, R., Costa, V., Sokolova, E. & Nistri, A. Modulation of neuronal nicotinic receptor function by the neuropeptides CGRP and substance P on autonomic nerve cells. *Br. J. Pharmacol.* **139**, 1061–1073 (2003).
39. Benemei, S., Nicoletti, P., Capone, J.A. & Geppetti, P. Pain pharmacology in migraine: focus on CGRP and CGRP receptors. *Neurol. Sci.* **28** (suppl. 2), S89–S93 (2007).
40. Disa, J., Parameswaran, N., Nambi, P. & Aiyar, N. Involvement of cAMP-dependent protein kinase and pertussis toxin–sensitive G-proteins in CGRP mediated JNK activation in human neuroblastoma cell line. *Neuropeptides* **34**, 229–233 (2000).
41. Borsello, T. & Forloni, G. JNK signalling: a possible target to prevent neurodegeneration. *Curr. Pharm. Des.* **13**, 1875–1886 (2007).
42. Perrin, V. *et al.* Implication of the JNK pathway in a rat model of Huntington's disease. *Exp. Neurol.* **215**, 191–200 (2009).
43. Mehan, S., Meena, H., Sharma, D. & Sankhla, R. JNK: a stress-activated protein kinase therapeutic strategies and involvement in Alzheimer's and various neurodegenerative abnormalities. *J. Mol. Neurosci.* **43**, 376–390 (2011).
44. Young, J.E. *et al.* Polyglutamine-expanded androgen receptor truncation fragments activate a Bax-dependent apoptotic cascade mediated by DP5/Hrk. *J. Neurosci.* **29**, 1987–1997 (2009).
45. Edvinsson, L. & Goadsby, P.J. Neuropeptides in migraine and cluster headache. *Cephalalgia* **14**, 320–327 (1994).
46. Katsuno, M. *et al.* for the Japan SBMA Interventional Trial for TAP-144-SR (JASMITT) study group. Efficacy and safety of leuprorelin in patients with spinal and bulbar muscular atrophy (JASMITT study): a multicentre, randomised, double-blind, placebo-controlled trial. *Lancet Neurol.* **9**, 875–884 (2010).
47. Fernández-Rhodes, L.E. *et al.* Efficacy and safety of dutasteride in patients with spinal and bulbar muscular atrophy: a randomised placebo-controlled trial. *Lancet Neurol.* **10**, 140–147 (2011).

ONLINE METHODS

Generation, maintenance and treatment of transgenic mice. We generated AR-24Q and AR-97Q male mice as previously described[11,48]. We used AR-97Q (Line #7-8) male mice because they show progressive muscular atrophy and weakness as well as SBMA-like pathology[25,49]. In the appropriate experiments, we administered naratriptan hydrochloride in drinking water (CAS No. 143388-64-1, Toronto Research Chemicals) to mice at a concentration of 1.8 or 18 μM in distilled water from 5 weeks of age until the end of the analysis, as described previously[14]. We performed castration or sham operations on male AR-97Q mice at the age of 5 weeks, as described previously[11,17]. We generated *Calca*-knockout mice (genetic background: 129/Sv × C57BL/6, backcrossed to C57BL/6) as previously described[50] and crossed them with the AR-97Q mice (genetic background: C57BL/6). We also used the littermates for phenotypic analyses. We used only males in this study. Background strain analyses using 96 genome-wide microsatellite markers (Aoba Genetics) demonstrated that the percentage of C57BL/6 was 99.2 ± 0.7% in the *Calca*-knockout mice used in this study. We performed all the animal experiments in accordance with the US National Institutes of Health Guide for the Care and Use of Laboratory Animals and under the approval of the Nagoya University Animal Experiment Committee.

Microarray analysis of mouse spinal cord. We analyzed alterations in gene expression using a GeneChip Mouse Genome 430 2.0 Array (Affymetrix) in male AR-97Q mice because they show a progressive motor dysfunction, muscle weakness and wasting, and they show histopathological evidence of the abnormal accumulation of the pathogenic AR within the nucleus of motor neurons, as is seen in patients with SBMA[22]. For each group (wild-type, AR-24Q and AR-97Q), we examined the male mice at 7–9, 10–12 and 13–15 weeks of age. We chose these stages because the AR-97Q mice are generally asymptomatic at 7–9 weeks of age (before-onset stage), present with mild motor impairment at 10–12 weeks (early stage) and are severely weakened with profound muscle atrophy at 13–15 weeks (advanced stage). RNA from the total spinal cord, excluding the dorsal root ganglia, was isolated from three mice of each genotype at each stage using Trizol reagent (Invitrogen) according to the manufacturer's specifications. The RNA samples were purified over RNeasy columns (Qiagen). TAKARA BIO performed the cDNA preparation, hybridization process and microarray data analysis (GEO accession GSE39865). The probe sets were extracted by the present detection call. We normalized the signals by the trimmed mean method and identified significantly different probe sets ($P < 0.005$) among the strains of mice and stages with a two-way repeated ANOVA. The criterion used to detect the differences in gene expression was a 1.5-fold change.

Assessment of motor ability. We assessed rotarod performance weekly using an Economex Rotarod (Ugo Basile) as described previously[51]. To measure grip strength, the same examiner (M.M.) placed the mice on wire netting with a Grip Strength Meter (MK-380M, Muromachikikai) and pulled them. We performed three trials weekly and recorded the best performance of the grasping power for each mouse with the examiner blinded with respect to the genotype and treatments.

Retrograde FluoroGold neurotracer labeling. We anesthetized the mice with pentobarbital and made a small incision in the skin of the left calf to expose the gastrocnemius muscle. We injected a total volume of 4.5 μl of 2.5% FluoroGold solution (Biotium) in PBS into three different parts of the muscle (proximal, middle and distal) using a 10-μl Hamilton syringe. We removed spinal cords 44 h after FluoroGold administration and post-fixed them with 4% paraformaldehyde in phosphate buffer. We counted the total number of FluoroGold-labeled motor neurons in serial 30-μm spinal cord sections with an Axio Imager M1 (Carl Zeiss).

Hematological analyses of the AR-97Q mice. We collected the blood from the mice at the advanced stage (13–15 weeks) during the dissection performed for the immunohistochemistry and immunoblotting. We measured the ALT and creatinine levels in the serum of the treated mice with the Japan Society of Clinical Chemistry standardization method (MDH-UV method) and the enzymatic method of Mitsubishi Chemical Medicine, respectively.

Plasmids, cell culture and transfection. We isolated SH-SY5Y (American Type Culture Collection No. CRL-2266) mRNA with the RNeasy Mini Kit (Qiagen) and reverse transcribed to yield cDNA. We amplified human *CALCA* cDNA from the SH-SY5Y cDNA with the PrimeStar HS DNA polymerase (Takara Bio) and Takara PCR Thermal Cycler Dice (Takara Bio). We used the following primers: 5′-AGAGGTGTCATGGGCTTCCA-3′ and 5′-GTT GGCATTCTGGGGCATGC-3′. We determined the sequence of the amplified cDNA with a CEQ8000 device (Beckman Coulter). We then cloned the human *CALCA* cDNA into pcDNA3.1/V5-His-TOPO (Invitrogen). For the promoter assay, we transfected GoClone and the pGL4 Luciferase Reporter Vector encoding the *CALCA* promoter (SwitchGear Genomics) into SH-SY5Y cells stably expressing human AR-97Q with Lipofectamine 2000 (Invitrogen). We used the Steady-Glo Luciferase Assay System (Promega) for the measurement of expression with POWERSCAN 4 (DS Pharma Biomedical). The *CALCA* promoter genomic coordinates were chr11-: 14950336–14951268. We plated the wild-type SH-SY5Y cells and those stably expressing the human AR-24Q or AR-97Q and maintained them in DMEM/F12 medium containing 10% FBS with penicillin and streptomycin. We transfected the cells in each dish with the CGRP1 or mock vector using OPTI-MEM (Invitrogen) and Lipofectamine 2000 (Invitrogen) and then differentiated them in DMEM/F12 supplemented with 20 μM retinoic acid and 1 nM 5α-dihydrotestosterone. We added FCS (5%) to the medium for the cell viability assay, but no serum was used for the cell toxicity assay because of the properties of the LDH measurement. We transfected the cells with the CGRP1 vector on days 0 and 2 for the cell viability assay and on day 0 for the LDH assay. We performed both evaluations on day 4. We selected the CGRP1-transfected SH-SY5Y cells for immunoblotting by adding 500 μg ml^{-1} of the antibiotic G418 (Sigma-Aldrich) to the medium 2 d after transfection because of the low transfection efficiency of the cells. We used nontransfected SH-SY5Y cells as selection controls. By 2 weeks after the addition of G418, the control SH-SY5Y cells had died, and we extracted the protein from the surviving CGRP1-transfected SH-SY5Y cells. We isolated human truncated AR cDNAs containing 24 or 97 CAGs (1–645 bp and 1–864 bp, respectively) from pCR3.1-full-length AR-24Q or AR-97Q vector[49] and subcloned them into the pLenti6.3/V5-DEST vector (Invitrogen), of which V5 tag was switched with EmGFP isolated from pcDNA6.2/C-EmGFP-DEST vector (Invitrogen). We transfected 293FT cells (Invitrogen) with the lentivirus vectors using the Virapower lentiviral system (Invitrogen).

SiRNA. We transfected the SH-SY5Y cells stably expressing AR-97Q with the siRNA oligonucleotide duplex at a concentration of 10 nM using Lipofectamine RNAiMAX (Invitrogen), according to the manufacturer's instructions. For knockdown of *CALCA*, we used the following oligonucleotide siRNA duplexes (Takara Bio) to transfect the SH-SY5Y AR-97Q stable cell line: against *CALCA*, sense sequence GUAAUCUGAGUACUUGCA UTT, antisense sequence AUGCAAGUACUCAGAUUACTT; control, sense sequence UCUUAAUCGCGUAUAAGGCTT, antisense sequence GCCUUAUACGCGAUUAAGATT. For knock-down of *DUSP1*, we used the following oligonucleotide siRNA duplexes (Stealth RNAi) to transfect the SH-SY5Y AR-97Q stable cell line: against *DUSP1* (1), sense sequence GACA UGCUGGAUGCCUUGGGCAUAA, antisense sequence UUAUGCCCAAG GCAUCCAGCAUGUC; against *DUSP1* (2), sense sequence GCCAUUGAC UUCAUAGACUCCAUCA, antisense sequence UGAUGGAGUCUAUGAA GUCAAUGGC. We used Stealth RNAi negative control duplex (Invitrogen) as the control for *DUSP1* siRNA.

Primary motor neuron culture. We dissected the spinal cord from C57BL/6 mouse embryos at E13. After removing meninges, dorsal root ganglia and the dorsal half of the spinal cord, we dissociated ventral part tissue into a single-cell suspension by Sumilon dissociation solution (Sumitomo Bakelite). We plated the cells at a density of 2×10^5 cells in a 24-well culture plate with Sumilon nerve-culture medium (Sumitomo Bakelite). On day 4, we infected the neurons with 3×10^5 copies μl^{-1} of lentivirus expressing truncated human AR with 24Q or 97Q[17]. After 3 h of infection, we removed the virus medium. We then cultured the neurons for 3 additional days and harvested them on day 7 followed by RNA extraction, cDNA synthesis, protein extraction, viability assay and immunocytochemistry.

Cell viability and toxicity assays. We performed the cell viability and LDH assays using WST-1 (Roche Diagnostics, Mannheim) and the Cytotoxicity Detection Kit PLUS (Roche Diagnostics), according to the manufacturer's instructions. We determined the number of dead cells using a Countess cell counter (Invitrogen) after staining with Trypan blue. We cultured the cells in 24-well plates. After each treatment, we incubated the cells with the WST-1 substrate for 3–4 h and spectrophotometrically assayed them at 440 nm using a plate reader (Powerscan HT, Dainippon Pharmaceutical). For the toxicity assays, we plated the wild-type SH-SY5Y cells and those stably expressing AR-97Q in the same medium used before transfection. The next day, we differentiated the cells in DMEM/F12 with the same supplement used after transfection. We administered the CGRP1 peptide and the CGRP1 antagonist, CGRP-1 8–37 (Peptide Institute), to the wild-type SH-SY5Y cells and those stably expressing AR-97Q in a serum-free medium for 3 d after differentiation. Two hours after treatment, we performed the cell viability assay. We also administered naratriptan hydrochloride (CAS No. 143388-64-1, Toronto Research Chemicals), rizatriptan benzoate (CAS No. 145202-66-0, Toronto Research Chemicals), sumatriptan succinate (CAS No. 103628-48-4, LKT Laboratories), SP-600125 (Merck), DUSP1 inhibitor (1 μM, Ro-31-8220, Calbiochem) and 5-HT inhibitor methiothepin mesylate (1 μM, sc-253005) in serum-free medium 3 d after differentiation. We administered naratriptan and other triptans at a concentration of 10 μM, unless otherwise mentioned. We performed the cell viability and cytotoxicity assays 24 h after drug administration.

Immunohistochemistry. We deeply anesthetized the mice and removed the entire spinal cord and skeletal muscles. We embedded the mouse samples and the autopsy specimens of the human lumbar spinal cord in paraffin[17] and performed immunohistochemistry and H&E staining as described previously[47,52]. We photographed the immunohistochemical sections with an optical microscope (Axio Imager M1, Carl Zeiss AG, Göttingen, Germany). For blocking/competition, we combined antibody (sc-8856, Santa Cruz, 1:50) with a fivefold (by weight) excess of blocking peptide (Peptide Institute). We obtained the autopsy specimens of the lumbar spinal cord from genetically diagnosed subjects with SBMA (52- and 77-year-old males) and from neurologically normal subjects (53- and 75-year-old males). The Ethics Committee of Nagoya University Graduate School of Medicine approved the collection of human tissues and their use in this study, and we obtained the written informed consent from the subjects' next of kin. We prepared 6-μm-thick sections from paraffin-embedded tissues and used the following primary antibodies: CGRP1 (sc-8856, Santa Cruz, 1:50); p-c-Jun (2361, Cell Signaling Technology, 1:100); c-Jun (#9165, Cell Signaling Technology, 1:400); GFAP (#2301-1, Epitomics, 1:250); and choline acetyltransferase (ab68779, Abcam, 1:1,000). Primary antibody binding was probed with a secondary antibody labeled with a polymer as part of the Envision+ system containing horseradish peroxidase (Dako). We measured the immunoreactivity of CGRP1 in the spinal motor neurons of SBMA and control subjects within five nonconsecutive sections with an interval of 30 μm from three subjects of each group. For the purposes of counting, we defined a motor neuron by its presence within the anterior horn and the obvious nucleolus in a given 6-μm-thick section. We calculated the intensities by multiplying the staining concentration by cell sizes using WinROOF (Mitani). We measured the immunoreactivity of p-c-Jun in more than 20 neurons within three nonconsecutive sections from each mouse ($n = 6$). For the purposes of counting, we defined a motor neuron as described above. We quantified the intensities and cell sizes with WinROOF. The means ± s.e.m. were expressed in arbitrary units.

Immunocytochemistry. We fixed mouse primary motor neurons with 4% paraformaldehyde, treated with 5% Triton X-100 and incubated them with the following primary antibodies: neurofilament H (SMI32, Covance, 1:500), GFP (598 or M048-3, MBL, 1:500) and p-c-Jun (2361, Cell Signaling Technology, 1:500).

Immunoblotting. We deeply anesthetized the mice with pentobarbital anesthesia, dissected the tissues (whole brains, spinal cords, brainstems and skeletal muscles), snap-froze them with powdered CO_2 in acetone and homogenized them in PhosphoSafe Extraction Reagent (Merck Chemicals) containing phosphatase inhibitor and HALT, which is a protease inhibitor cocktail (Thermo Scientific). We lysed the cultured cells in the same reagent after intervention. We used NE-PER Nuclear Cytoplasmic Reagents (Thermo Scientific) for the analysis of the NF-κB pathway. We separated the samples on 5–20% SDS-PAGE gels and then transferred them to Hybond-P membranes (GE Healthcare) using 25 mM Tris, 192 mM glycine, 0.1% SDS and 10% methanol as the transfer buffer. We diluted the primary and secondary antibodies with Can Get Signal, which is a signal enhancer solution (NKB-101, Toyobo). We digitized the immunoblots with an LAS-3000 imaging system (Fujifilm), quantified the signal intensities of the independent blots with Image Gauge software, version 4.22 (Fujifilm), and expressed the means ± s.e.m. in arbitrary units. We used the following primary antibodies: p-c-Jun (#2361, Cell Signaling Technology, 1:1,000); c-Jun (ab16777, Abcam, 1:40); p-JNK (NB110-66666, Novus Biologicals, 1:1,000); JNK (#9252, Cell Signaling Technology, 1:1,000); choline acetyltransferase (ab68779, Abcam, 1:1,000); DUSP1 (sc-1199, Santa Cruz, 1:100); p-NFKBIA (#9241, Cell Signaling Technology, 1:1,000); NFKBIA (#1130-1, Epitomics, 1:10,000); NF-κB p65 (sc-8008, Santa Cruz, 1:200); NF-κB p50 (sc-8414, Santa Cruz, 1:200); histone H1 (sc-8030, Santa Cruz, 1:100); α-tubulin (T5168, Sigma-Aldrich, 1:5000); phospho-ERK1/2 (4370, Cell Signaling Technology, 1:2,000); and ERK1/2 (#4695, Cell Signaling Technology, 1:1,000). We probed the primary antibody binding using horseradish peroxidase–conjugated secondary antibodies (GE Healthcare) at a dilution of 1:5,000, and detected the bands using the ECL Plus kit (GE Healthcare).

Quantitative real-time PCR. We determined the mRNA levels of the examined genes by real-time PCR as described previously[15,52]. Briefly, we extracted total RNA from the mouse spinal cords using TRIzol Reagent (Invitrogen) and from the cells using the RNeasy Mini Kit (Qiagen). We then reverse transcribed the extracted RNA into first-strand cDNA using SuperScript III reverse transcriptase (Invitrogen). We performed real-time PCR in a total volume of 50 μl that contained 25 μl 2× QuantiTect SYBR Green PCR Master Mix and 0.4 μM of each primer (Qiagen), and we detected the amplified products by the iCycler system (Bio-Rad Laboratories). The reaction conditions were 95 °C for 15 min, followed by 45 cycles of 15 s at 95 °C, 30 s at 55 °C and 30 s at 72 °C. As an internal control, we simultaneously quantified the expression level of glyceraldehyde-3-phosphate dehydrogenase (*GAPDH*). We used the following primers: 5′-GAAGAAGAAGTTCGCCTGCT-3′ and 5′-GATTCCCACACCGCTTAGAT-3′ for mouse *Calca*, 5′-CCTGGAGAAACCTGCCAAGTAT-3′ and 5′-TGAAGTCGCAGGAGACAACCT-3′ for mouse *Gapdh*, 5′-ACTGGTGCAGGACTATGTGC-3′ and 5′-CTTGTTGAAGTCCTGCGTGT-3′ for human *CALCA*, and 5′-AGCCTCAAGATCATCAGCAAT-3′ and 5′-GGACTGTGGTCATGAGTCCTT-3′ for human *GAPDH*. The weight of the gene contained in each sample was equal to the log of the starting quantity, and the standardized expression level of each mouse was equal to the weight ratio of each gene to that of *Gapdh*. We repeated the PCRs three times for each of the indicated numbers of samples.

ELISA. We extracted the lysates of the SH-SY5Y cells stably expressing AR-24Q and AR-97Q with CelLytic-M (Sigma-Aldrich) after each intervention. We used the CGRP EIA kit (Phoenix Pharmaceuticals), and corrected the loading dose with a PathScan Total α-Tubulin Sandwitch Elisa Kit (Cell Signaling Technology).

Statistical analyses. We analyzed the data using the Kaplan-Meier and log-rank tests for the survival rate, the unpaired *t*-test for two-group comparisons, and ANOVA with Dunnett's or Tukey's *post hoc* tests for multiple comparisons. We performed the statistical analyses using Statview software version 5 (HULINKS) and Prism version 4 (GraphPad Software).

48. Niwa, H., Yamamura, K. & Miyazaki, J. Efficient selection for high-expression transfectants with a novel eukaryotic vector. *Gene* **108**, 193–199 (1991).
49. Waza, M. *et al.* 17-AAG, an Hsp90 inhibitor, ameliorates polyglutamine-mediated motor neuron degeneration. *Nat. Med.* **11**, 1088–1095 (2005).
50. Oh-hashi, Y. *et al.* Elevated sympathetic nervous activity in mice deficient in alphaCGRP. *Circ. Res.* **89**, 983–990 (2001).
51. Adachi, H. *et al.* CHIP overexpression reduces mutant androgen receptor protein and ameliorates phenotypes of the spinal and bulbar muscular atrophy transgenic mouse model. *J. Neurosci.* **27**, 5115–5126 (2007).
52. Tokui, K. *et al.* 17-DMAG ameliorates polyglutamine-mediated motor neuron degeneration through well-preserved proteasome function in an SBMA model mouse. *Hum. Mol. Genet.* **18**, 898–910 (2009).

nature medicine

Viral delivery of miR-196a ameliorates the SBMA phenotype via the silencing of CELF2

Yu Miyazaki[1], Hiroaki Adachi[1], Masahisa Katsuno[1], Makoto Minamiyama[1], Yue-Mei Jiang[1], Zhe Huang[1], Hideki Doi[1], Shinjiro Matsumoto[1], Naohide Kondo[1], Madoka Iida[1], Genki Tohnai[1], Fumiaki Tanaka[1], Shin-ichi Muramatsu[2] & Gen Sobue[1]

Spinal and bulbar muscular atrophy (SBMA) is an inherited neurodegenerative disorder caused by the expansion of the polyglutamine (polyQ) tract of the androgen receptor (AR-polyQ)[1,2]. Characteristics of SBMA include proximal muscular atrophy, weakness, contraction fasciculation and bulbar involvement[3]. MicroRNAs (miRNAs) are a diverse class of highly conserved small RNA molecules that function as crucial regulators of gene expression in animals and plants[4]. Recent functional studies have shown the potent activity of specific miRNAs as disease modifiers both *in vitro* and *in vivo*[5–8]. Thus, potential therapeutic approaches that target the miRNA processing pathway have recently attracted attention[9,10]. Here we describe a novel therapeutic approach using the adeno-associated virus (AAV) vector–mediated delivery of a specific miRNA for SBMA. We found that miR-196a enhanced the decay of the AR mRNA by silencing CUGBP, Elav-like family member 2 (CELF2). CELF2 directly acted on AR mRNA and enhanced the stability of AR mRNA. Furthermore, we found that the early intervention of miR-196a delivered by an AAV vector ameliorated the SBMA phenotypes in a mouse model. Our results establish the proof of principle that disease-specific miRNA delivery could be useful in neurodegenerative diseases.

A mouse model of SBMA has been developed[11], and several therapeutic approaches for SBMA have been presented using this mouse model[11–15]. Among these approaches, the reduction of mutant AR protein levels in male mice ameliorated disease manifestations, suggesting a potential therapy for SBMA. miRNAs guide the RNA-induced silencing complex to mRNAs that have a target sequence complementary to that of the miRNA. The interaction between the miRNA and the target can occur with an incomplete complementary sequence; thus, a single miRNA can modulate complex physiological functions or disease phenotypes by regulating widespread networks[16]. Over the last several years, an important role of miRNAs in the pathogenesis of neurodegenerative disorders has been reported[5–8,17,18].

In this study, we used a miRNA microarray analysis to compare the miRNA expression in the spinal cords of male transgenic SBMA model mice expressing full-length human AR with 97 glutamine residues (AR-97Q) and in male mice expressing wild-type human AR (AR-24Q)[11]. Of more than 500 miRNAs tested, miR-196a (accession number MIMAT_0000518), miR-196b (accession number MIMAT_0001081), miR-496 (accession number MIMAT_0003738), miR miR-323-3p (accession number MIMAT_0000551) and miR-29b* (accession number MIMAT_0004523) showed a greater than two-fold upregulation in the spinal cord of AR-97Q mice at an advanced disease stage relative to the AR-24Q mice (**Fig. 1a**).

To examine the effects of these five miRNAs on the expression levels of AR mRNA transcribed from the *AR* gene, we co-transfected synthetic miRNAs with vectors expressing human AR-24Q or AR-97Q into HEK293T cells. Among these five miRNAs, miR-196a and miR-196b downregulated the AR mRNA and protein (**Fig. 1b,c**), although the transgene used in both the *in vitro* and *in vivo* experiments lacked the DNA sequence that encodes the AR mRNA 3′ untranslated region (UTR) (**Supplementary Fig. 1**). To determine whether the decrease in the AR mRNA level was due to the enhancement of mRNA degradation or a decrease in mRNA synthesis, we assessed the turnover of AR mRNA using an RNA stability assay with actinomycin D. In the absence of miR-196a and miR-196b, the AR mRNA had a half-life of >1.5 h. The AR mRNA had a half-life of <0.5 h in the presence of miR-196a and miR-196b (**Fig. 1d**). These findings indicated that miR-196a and miR-196b enhanced the degradation of AR mRNA via an interaction with cofactors that were able to stabilize both the wild-type and mutant AR mRNAs.

To elucidate the molecular mechanisms by which miR-196a and miR-196b regulate the stability of AR mRNA, we analyzed their potential targets using the bioinformatics program TargetScan Release 6.0. Among the hundreds of mRNAs targeted by miR-196a and miR-196b, CELF2 mRNA has a common binding site for miR-196a and miR-196b that is broadly conserved among vertebrates (**Supplementary Fig. 2**). We found that CELF2 mRNA and protein levels were significantly reduced by treatment with miR-196a and miR-196b in HEK293T cells (**Fig. 1e**) and that CELF2 was required for AR mRNA stability

[1]Department of Neurology, Nagoya University Graduate School of Medicine, Nagoya, Japan. [2]Division of Neurology, Department of Medicine, Jichi Medical University, Tochigi, Japan. Correspondence should be addressed to G.S. (sobueg@med.nagoya-u.ac.jp).

Received 3 October 2011; accepted 18 April 2012; published online 3 June 2012; doi:10.1038/nm.2791

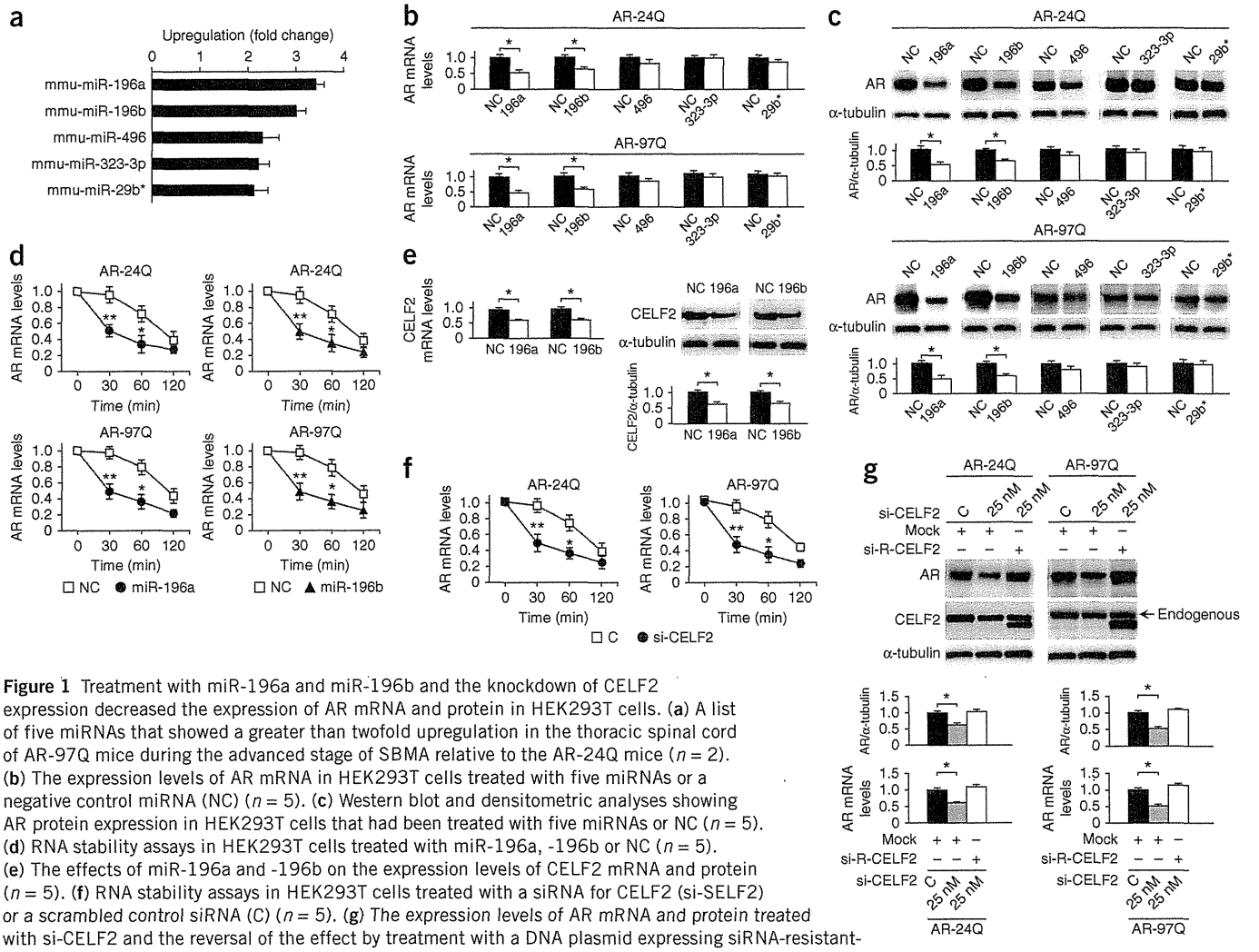

Figure 1 Treatment with miR-196a and miR-196b and the knockdown of CELF2 expression decreased the expression of AR mRNA and protein in HEK293T cells. (**a**) A list of five miRNAs that showed a greater than twofold upregulation in the thoracic spinal cord of AR-97Q mice during the advanced stage of SBMA relative to the AR-24Q mice ($n = 2$). (**b**) The expression levels of AR mRNA in HEK293T cells treated with five miRNAs or a negative control miRNA (NC) ($n = 5$). (**c**) Western blot and densitometric analyses showing AR protein expression in HEK293T cells that had been treated with five miRNAs or NC ($n = 5$). (**d**) RNA stability assays in HEK293T cells treated with miR-196a, -196b or NC ($n = 5$). (**e**) The effects of miR-196a and -196b on the expression levels of CELF2 mRNA and protein ($n = 5$). (**f**) RNA stability assays in HEK293T cells treated with a siRNA for CELF2 (si-SELF2) or a scrambled control siRNA (C) ($n = 5$). (**g**) The expression levels of AR mRNA and protein treated with si-CELF2 and the reversal of the effect by treatment with a DNA plasmid expressing siRNA-resistant-CELF2 (si-R-CELF2) ($n = 5$). All data are means ± s.e.m. $^*P < 0.05$ and $^{**}P < 0.01$. We analyzed the results by unpaired *t* tests in **b**, **c** and **e**; by two-way ANOVA followed by the Bonferroni test comparing HEK293T cells treated with miR-196a or miR-196b to cells treated with NC in **d**; by two-way ANOVA followed by the Bonferroni test comparing HEK293T cells treated with si-CELF2 to cells treated with control siRNA in **f**; and by the Dunnett test in **g**.

(**Fig. 1f**). The knockdown of CELF2 expression with specific small interfering RNAs (siRNAs) silenced CELF2 protein, accelerated the degradation of AR mRNA and led to a decrease in AR protein expression levels (**Fig. 1g**). These downregulating effects were reversed in rescue experiments using a DNA plasmid that expressed siRNA-resistant CELF2, thus confirming the interaction between CELF2 and AR mRNA (**Fig. 1g**). In contrast to the knockdown and rescue results, the overexpression of CELF2 increased the expression levels of AR mRNA and protein (**Fig. 2a**) and increased the stability of the AR mRNA (**Fig. 2b**). To determine the region of the AR mRNA that interacts with CELF2, we prepared several constructs of the mutated *AR* transgene that lacked the CAG repeats (AR-0Q) or the three triplet repeats of the CUGCUGCUG sequence (ΔCUG-AR-24Q and ΔCUG-AR-97Q), which is immediately proximal to the CAG repeats in exon 1 of the AR mRNA and is conserved in the endogenous human AR mRNA (**Fig. 2c**). Although the overexpression of CELF2 increased the expression levels of AR mRNA and protein transcribed from the mutated transgene lacking CAG repeats, the expression levels of AR mRNA and protein transcribed from the mutated transgene lacking the three triplet repeats of the CUGCUGCUG sequence were not increased relative to controls by CELF2 (**Fig. 2d**). In addition, immunoprecipitation-coupled quantitative real time-PCR (qRT-PCR) revealed the binding affinity of CELF2 to the three triplet repeats of the CUGCUGCUG sequence in exon 1 of the AR mRNA (**Fig. 2e**). On the basis of these findings, we concluded that miR-196a and miR-196b were able to decrease the expression levels of AR mRNA and protein by silencing CELF2, a protein that enhances the stability of AR mRNA through direct binding to the CUG triplet repeat sequence in exon 1 of the AR mRNA.

To examine the effects of CELF2 silencing on the motor impairment of SBMA mice, we constructed an *in vivo* delivery system based on an AAV vector that allowed for the simultaneous expression of enhanced green fluorescent protein (EGFP) and either miR-196a (AAV-miR-196a) or a nonspecific miRNA, miR-mock (AAV-miR-mock). We chose to use miR-196a instead of miR-196b because the expression of miR-196a was highly upregulated in the cytoplasm of the motor neurons of AR-97Q mice (**Supplementary Fig. 3**). A viral load of 10^{11} vector genomes (vg) of each of these constructs was injected into the skeletal muscle of the left quadriceps femoris of AR-97Q mice. The AAV vector can be transported efficiently in a retrograde manner from muscle to the motor neurons of the spinal cord[19,20] and can spread hematogenously[21,22]. Two weeks after AAV vector injection,

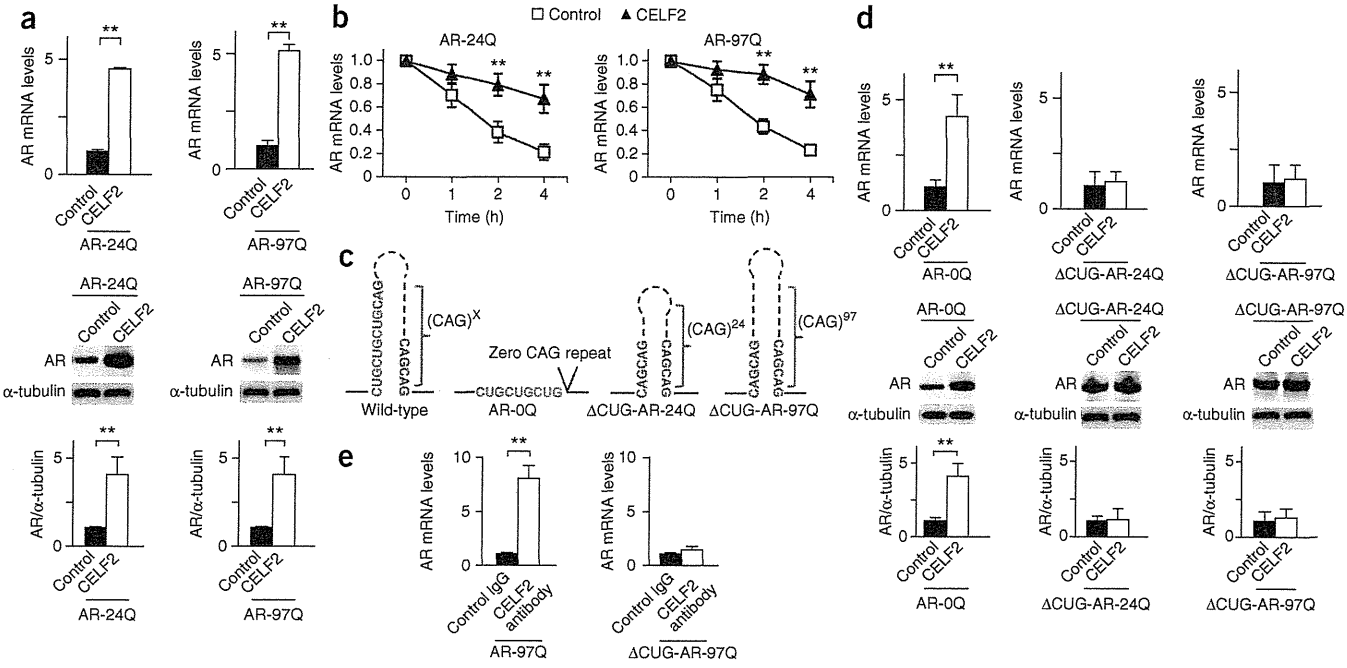

Figure 2 CELF2 recognizes the sequence CUGCUGCUG in exon 1 of the AR mRNA and increases the stability of the AR mRNA. (**a**) The expression levels of AR mRNA and protein in HEK293T cells treated with the DNA plasmid expressing human CELF2 (CELF2) or the original pcDNA3.1/HisC vector (control) ($n = 5$). (**b**) RNA stability assays in HEK293T cells treated with CELF2 or control ($n = 5$). (**c**) Schematic diagrams of the AR mRNA structure near the hairpin loop of the CAG repeats (red) transcribed from wild-type and mutated DNA plasmids. AR-0Q lacks the CAG repeats, and ΔCUG-AR-24Q and ΔCUG-AR-97Q lack the sequence CUGCUGCUG (blue) immediately adjacent to the CAG repeats. (**d**) AR mRNA and protein expression levels in HEK293T cells co-transfected with CELF2 and the mutated DNA plasmids expressing AR ($n = 5$). (**e**) The amount of AR-97Q and ΔCUG-AR-97Q mRNA binding to CELF2 that was immunoprecipitated using an antibody against CELF2 or a control immunoglobulin (IgG) ($n = 5$). All data are means ± s.e.m. $^{**}P < 0.01$ (we analyzed the results by unpaired *t* tests in **a**,**d** and **e** and by two-way ANOVA followed by the Bonferroni test comparing HEK293T cells treated with CELF2 to cells treated with control in **b**).

a widespread transduction of the viral particles throughout the brain, spinal cord and the skeletal muscle of the upper and lower limbs was observed (**Supplementary Fig. 4a**). There was no difference in the expression of EGFP between the left and right sides of the spinal cord (**Supplementary Fig. 4b**). The presence of the AAV vector in the motor neurons of infected mice was visually confirmed by the colocalization of EGFP and staining for choline acetyltransferase (ChAT), a motor neuron marker (**Supplementary Fig. 4c**). Because the widespread viral transduction throughout the entire body was also detected in mice in which virus was injected into a cardiac chamber (**Supplementary Fig. 4d**), we deduced that the viral particles injected into the hind limb skeletal muscle spread hematogenously throughout the entire body of the mouse. In addition to viral distribution, a tyrosine mutation of the adeno-associated viral capsid protein may contribute to the enhanced transgene expression levels delivered by AAV[23]. We then did an AAV vector injection into the quadriceps femoris of a 5-week-old mouse, before the onset of motor impairment in the SBMA mice (approximately 7 weeks of age), because transgene expression stabilizes approximately 2 weeks after vector delivery.

The disease progression in the AR-97Q mice treated with AAV-miR-196a (AR-97Q-miR-196a mice) was ameliorated compared with AAV-miR-mock-treated mice. The AR-97Q mice treated with AAV-miR-mock (AR-97Q-miR-mock mice) showed motor impairment, as assessed by the rotarod task, as early as 7 weeks after birth. By contrast, the AR-97Q-miR-196a mice showed an initial impairment at 13 weeks after birth but showed less deterioration than their AR-97Q-miR-mock counterparts ($P < 0.001$) (**Fig. 3a**). The locomotor cage activity of the AR-97Q-miR-mock mice was also markedly decreased at 7 weeks compared with that of the AR-97Q-miR-196a mice ($P < 0.001$), which showed decreased activity at 13 weeks of age (**Fig. 3b**). Moreover, the AR-97Q-miR-mock mice lost weight significantly earlier and more profoundly than the AR-97Q-miR-196a mice ($P < 0.001$) (**Fig. 3c**). Treatment with miR-196a significantly prolonged the survival of the AR-97Q-miR-196a mice ($P < 0.001$) compared with the AR-97Q-miR-mock mice (**Fig. 3d**). By 12 weeks of age, the AR-97Q-miR-mock mice showed obvious differences in body size, muscular atrophy and kyphosis compared with the AR-97Q-miR-196a mice (**Fig. 3e**). In addition, the AR-97Q-miR-mock mice showed motor weakness, as indicated by short steps and leg dragging, whereas the AR-97Q-miR-196a mice showed almost normal ambulation (**Fig. 3f**). Immunohistochemical examination of mouse tissues using 1C2 antibody, which specifically recognizes the expanded polyQ region in the mutant AR, showed a marked reduction in 1C2-positive nuclear accumulation in the anterior horn of the thoracic spinal cord and in the skeletal muscles of the right quadriceps femoris of the AR-97Q-miR-196a mice compared with those of the AR-97Q-miR-mock mice. Glial fibrillary acidic protein (GFAP)-specific antibody staining showed that the AAV vector–mediated delivery of miR-196a reduced reactive astrogliosis in the thoracic spinal anterior horn of the AR-97Q mice, thereby suggesting that miR-196a attenuated neurodegenerative changes. Histopathological examination of the skeletal muscle showed marked amelioration of neurogenic muscle atrophy in the AR-97Q-miR-196a mice compared with the AR-97Q-miR-mock mice (**Fig. 3g**). By quantitative assessment, we confirmed that AAV-miR-196a significantly reduced 1C2-positive nuclear accumulation in the anterior horn of the thoracic spinal cord ($P < 0.01$) and

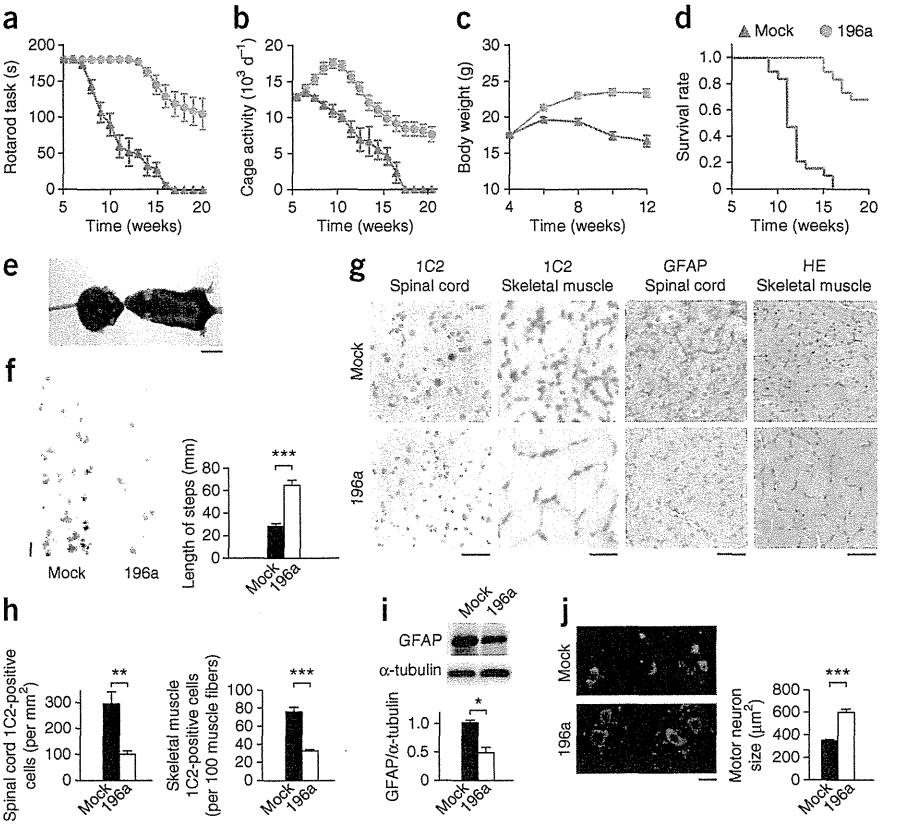

Figure 3 The effects of miR-196a on the phenotype of male AR-97Q mice. (**a–d**) A rotarod task (**a**), cage activity (**b**), body weight (**c**) and survival rate (Kaplan-Meier analysis and log-rank test) (**d**) of the AR-97Q-miR-mock (mock) or AR-97Q-miR-196a mice (196a) ($n = 19$ in each group). $P < 0.001$ for all data at each time after 8 weeks of age in **a–c**. (**e**,**f**) A representative photograph (**e**) and footprints (**f**) of a 12-week-old AR-97Q-miR-mock mouse (left) and an age-matched AR-97Q-miR-196a mouse (right). The front and hind paws are indicated in red and blue, respectively. Each column shows the average length of the steps taken by the hind paw ($n = 5$). Scale bars, 20 mm. (**g**) Immunohistochemical staining for the mutant AR using the 1C2 antibody of the thoracic spinal cord and skeletal muscle of the right quadriceps femoris; immunohistochemical staining with a GFAP-specific antibody of the thoracic spinal anterior horn; and hematoxylin and eosin (HE) staining of the skeletal muscle of the right quadriceps femoris. Scale bars, left to right: 50 μm, 10 μm, 50 μm, 20 μm. (**h**) Quantification of 1C2-positive cells in the thoracic spinal cord and skeletal muscle of the right quadriceps femoris ($n = 5$). (**i**) Western blot and densitometric analyses showing the levels of GFAP protein expression in the thoracic spinal cord ($n = 5$). (**j**) The mean size of the motor neurons of the thoracic spinal cord obtained from AR-97Q-miR-196a mice compared with that of AR-97Q-miR-mock mice ($n = 5$). Scale bar, 20 μm. All data are means ± s.e.m. $^*P < 0.05$, $^{**}P < 0.01$ and $^{***}P < 0.001$ (we analyzed the results by two-way ANOVA followed by the Bonferroni test comparing the mock to 196a in **a–c** and by unpaired t test in **f**, **h–j**).

in the skeletal muscle of the right quadriceps femoris ($P < 0.001$) of the AR-97Q-mice (**Fig. 3h**). Western blot analyses and quantification of the immunohistochemical signal intensities revealed that treatment with miR-196a downregulated the expression levels of GFAP (**Fig. 3i** and **Supplementary Fig. 5**). In addition, treatment with miR-196a significantly suppressed motor neuron shrinkage ($P < 0.001$) (**Fig. 3j**).

At 3 weeks after injection of a viral load of 10^{11} vg, we killed the mice and harvested the RNA and protein in the thoracic spinal cord for analysis. The AR-97Q-miR-196a mice showed high expression levels of miR-196a and low expression levels of CELF2 mRNA, mutant AR mRNA and the endogenous mouse AR mRNA in the thoracic spinal cord compared with AR-97Q-miR-mock mice (**Fig. 4a**). The mouse AR mRNA lacks a CUGCUGCUG tract; however, it has the CUGCUG sequence in its coding region that would interact with CELF2. Western blotting analyses of thoracic spinal cord lysates of the AR-97Q-miR-mock mice showed that the high-molecular-weight mutant AR protein complex was retained in the stacking gel and that a monomeric AR migrated as a band through the separating gel (**Fig. 4b**). Treatment with AAV-miR-196a notably reduced both the high-molecular-weight complex and the monomer of AR and CELF2 in the thoracic spinal cord (**Fig. 4b**). We observed the elevated expression levels of miR-196a achieved by AAV vector–mediated expression and the decreased expression levels of mutant AR mRNA in the thoracic spinal cord throughout the follow-up period of 15 weeks (**Fig. 4c**). Although we detected the effects of the miR-196a treatment in the skeletal muscle, we found that the increase in the levels of miR-196a expression and the downregulation of mutant AR mRNA and protein were more prominent in the spinal cord than in the skeletal muscle (**Supplementary Fig. 6**). The skeletal muscle of the right quadriceps femoris, contralateral to the site of the AAV vector injection, also showed treatment effects (**Supplementary Fig. 6**). AR-97Q-miR-196a mice showed no detectable reduction in the normal serum testosterone levels, which has been shown to directly affect the levels of AR expression (**Fig. 4d**)[11].

To address whether miR-196a-mediated treatment can be useful in the therapy of patients with SBMA, we examined the effects of miR-196a on AR mRNA and protein in fibroblasts obtained from patients with SBMA and from disease control subjects. Treatment with miR-196a downregulated both the AR and CELF2 mRNAs and proteins in the fibroblasts obtained from patients with SBMA (**Fig. 4e**) and disease control subjects (**Supplementary Fig. 7**). We also observed similar effects for AR mRNA and protein in fibroblasts treated with CELF2 siRNA (**Fig. 4f**). Taken together, these findings suggest that miR-196a-mediated treatment might be useful in the therapy of patients with SBMA. Furthermore, we measured the expression levels of miR-196a, miR-196b and CELF2 mRNA in the thoracic spinal cord of patients with SBMA. Both of the two miRNAs were upregulated and the CELF2 mRNA was downregulated in the thoracic spinal cord of patients with SBMA compared with those of disease control subjects (**Fig. 4g**). qRT-PCR revealed that the expression levels of CELF2 mRNA were lower in the thoracic spinal cord of AR-97Q mice than in AR-24Q mice (**Supplementary Fig. 8**), thereby confirming the correlations between the *in vivo* levels of the two miRNAs and CELF2 mRNA. We also showed the *in vivo* correlation between miR-196a and mutant AR mRNA levels and monitored the side effects of mice treated with AAV-miR-196a (**Supplementary Note**

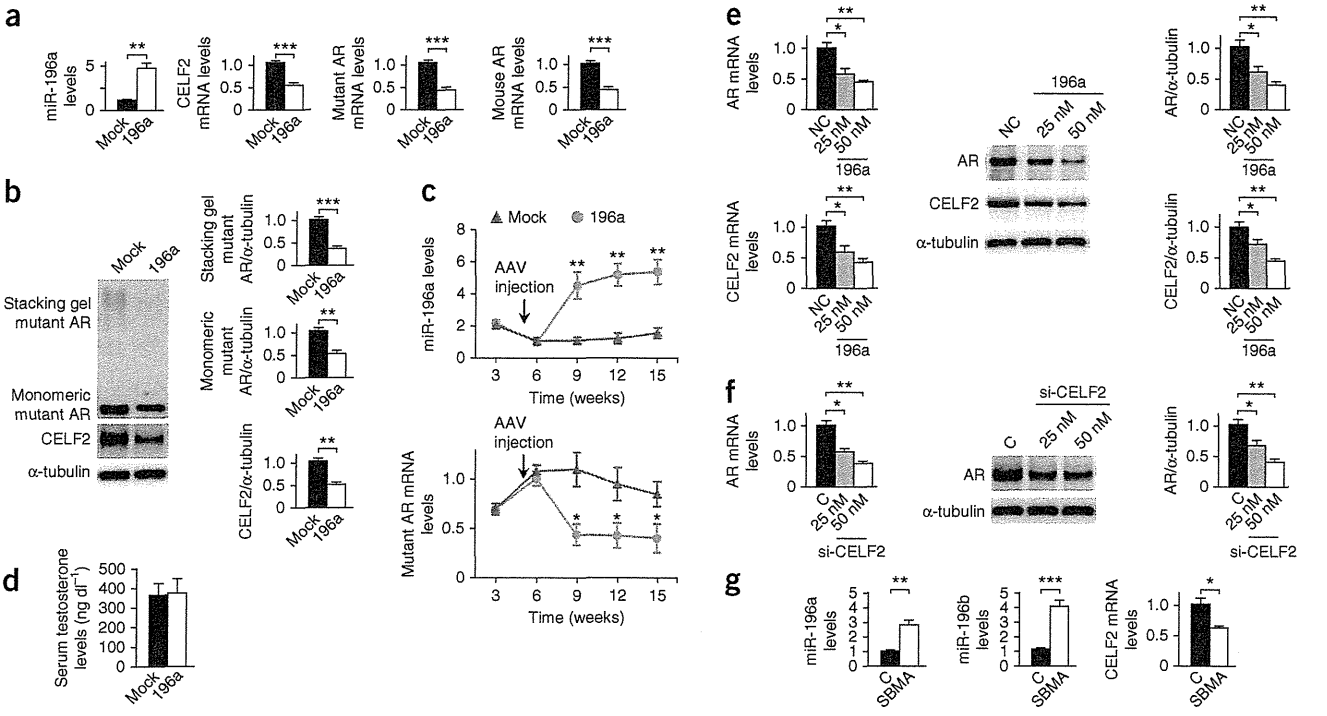

Figure 4 The effects of miR-196a on mutant AR expression in male AR-97Q mice and patients with SBMA. (**a**) The levels of miR-196a, CELF2 mRNA, mutant AR mRNA and the endogenous mouse AR mRNA expression in the thoracic spinal cord of AR-97Q-miR-mock (mock) and AR-97Q-miR-196a (196a) mice ($n = 5$). (**b**) Western blot and densitometric analyses showing the expression levels of mutant AR both in the stacking and separating gels as well as those of CELF2 ($n = 5$). (**c**) A temporal change in the levels of miR-196a and mutant AR mRNA expression in the thoracic spinal cord of AR-97Q-miR-mock and AR-97Q-miR-196a mice ($n = 3$ to 4). (**d**) The serum testosterone levels of AR-97Q-miR-mock and AR-97Q-miR-196a mice ($n = 5$). (**e**) The expression levels of mutant AR mRNA, CELF2 mRNAs and their proteins in the fibroblasts of patients with SBMA ($n = 5$). NC, a negative control miRNA. (**f**) The effects of CELF2 silencing on mutant AR mRNA and protein in the fibroblasts of patients with SBMA ($n = 5$). C, a scrambled control siRNA. (**g**) The expression levels of miR-196a, -196b and CELF2 mRNA in the thoracic spinal cord of patients with SBMA ($n = 3$). C, disease control subjects. All data are means ± s.e.m. $^*P < 0.05$, $^{**}P < 0.01$ and $^{***}P < 0.001$ (we analyzed the results by unpaired t tests in **a**,**b**,**d** and **g** and by two-way ANOVA followed by the Bonferroni test comparing the mock to 196a in **c**, and by the Dunnett test in **e**,**f**).

and **Supplementary Fig. 8**). In addition, we examined the post-translational effects of miR-196a in HEK293T and the effects of miR-196a on apoptosis in Neuro2a cells (**Supplementary Note** and **Supplementary Fig. 9**). We also showed the effects of miR-196a downregulation on mutant AR mRNA and protein in HEK293T cells (**Supplementary Note** and **Supplementary Fig. 10**).

In this study, we showed that miR-196a is upregulated in the spinal cord of a transgenic mouse model of SBMA during the symptomatic stage and that early intervention by the transduction of mice with miR-196a via an AAV vector can markedly ameliorate the motor impairment of SBMA mice. We further showed that miR-196a silences CELF2, which then directly acts on AR mRNA to affect its stability. Although polyQ models have been shown to have altered miRNA profiles[7,17] and miRNAs targeting of the polyQ disease gene have been proposed as disease modifiers [6,7], the miRNA-mediated therapeutic approach targeting a regulator of the disease transcript described in our study is conceptually novel and could be strategically applied to other polyQ-related diseases.

The upregulation of miR-196a has been reported in a wide variety of cancers[24,25] and has also been shown to be involved in differentiation[26,27] and the development of the immune system[28]. Hence, miR-196a has previously been proposed as a therapeutic target for these ailments. Similarly, the modulation of CELF2 has known implications for myotonic dystrophy[29] and several cancer types[30,31].

Our results show that the strong and continuous inhibition of the expression of CELF2 by the AAV vector–mediated delivery of miR-196a has a substantial effect on the SBMA phenotype. Although the reason for the natural upregulation of miR-196a in the spinal cord of SBMA mice and patients with SBMA is unknown, it may indicate a protective mechanism that is insufficient alone but sufficiently beneficial when amplified by AAV-mediated overexpression. However, whether similarly effective therapy would result from injections to an isolated skeletal muscle in patients with SBMA must be verified. The appropriate route and the required dose of AAV administration should be determined in future studies. Our findings indicate that the miRNA-mediated regulation of RNA metabolism is a logical target for the therapeutic intervention of SBMA and they suggest a new therapeutic approach using an AAV vector–mediated miRNA delivery system for the treatment of neurodegenerative disease.

METHODS

Methods and any associated references are available in the online version of the paper.

Note: Supplementary information is available in the online version of the paper.

ACKNOWLEDGMENTS

We are grateful to T. Cooper (Department of Pathology and Immunology, Baylor College of Medicine) for kindly providing the plasmid expressing human CELF2. We also thank N. Takino, H. Miyauchi and K. Ayabe (Division of Neurology, Department of Medicine, Jichi Medical University) for their help with the production of the AAV vectors and Y. Kondo and K. Shinjo (Division of Molecular Oncology, Aichi Cancer Center Research Institute) for expert technical support and helpful discussions. This work was supported by grants from the Ministry of Health,